CAPITAL UNIVERSITY OF SCIENCE AND TECHNOLOGY, ISLAMABAD

Simulation of MHD Mixed Convection Nanofluid Flow in a Cavity with an Obstacle and Non-Linear Thermal Radiations

by

Rukhshanda Tariq

A thesis submitted in partial fulfillment for the degree of Master of Philosophy

in the

Faculty of Computing
Department of Mathematics

2018

This thesis is dedicated to my beloved mom, **Rubina Tariq** who always keeps me motivated and positive whenever I got fed up with this and wanted to quit, to my father, **Tariq Mahmood** for letting me reach at this level and finally to **Dr. Shafqat Hussain** for his patience throughout my work.

CAPITAL UNIVERSITY OF SCIENCE & TECHNOLOGY
ISLAMABAD

CERTIFICATE OF APPROVAL

Simulation of MHD Mixed Convection Nanofluid Flow in a Cavity with an Obstacle and Non-Linear Thermal Radiations

by

Rukhshanda Tariq
Registration No MMT163004

THESIS EXAMINING COMMITTEE

S. No.	Examiner	Name	Organization
(a)	External Examiner	Dr. Sadia Siddiqa	CUI, Attock Campus
(b)	Internal Examiner	Dr. Muhammad Afzal	CUST, Islamabad
(c)	Supervisor	Dr. Shafqat Hussain	CUST, Islamabad

Dr. Shafqat Hussain
Thesis Supervisor
October, 2018

Dr. Muhammad Sagheer
Head
Dept. of Mathematics
October, 2018

Dr. Muhammad Abdul Qadir
Dean
Faculty of Computing
October, 2018

Author's Declaration

I, **Rukhshanda Tariq** hereby state that my MS thesis titled "**Simulation of MHD Mixed Convection Nanofluid Flow in a Cavity with an Obstacle and Non-Linear Thermal Radiations**" is my own work and has not been submitted previously by me for taking any degree from Capital University of Science and Technology, Islamabad or anywhere else in the country/abroad.

At any time if my statement is found to be incorrect even after my graduation, the University has the right to withdraw my MPhill Degree.

(Rukhshanda Tariq)

Registration No: MMT163004

Plagiarism Undertaking

I solemnly declare that research work presented in this thesis titled "*Simulation of MHD Mixed Convection Nanofluid Flow in a Cavity with an Obstacle and Non-Linear Thermal Radiations*" is solely my research work with no significant contribution from any other person. Small contribution/help wherever taken has been dully acknowledged and that complete thesis has been written by me.

I understand the zero tolerance policy of the HEC and Capital University of Science and Technology towards plagiarism. Therefore, I as an author of the above titled thesis declare that no portion of my thesis has been plagiarized and any material used as reference is properly referred/cited.

I undertake that if I am found guilty of any formal plagiarism in the above titled thesis even after award of MPhill degree, the University reserves the right to withdraw/revoke my MPhill degree and that HEC and the University have the right to publish my name on the HEC/University website on which names of students are placed who submitted plagiarized work.

(Rukhshanda Tariq)

Registration No: MMT163004

Acknowledgements

Starting with the name of Almighty **ALLAH** who is most gracious and omnipresent, who makes the mankind and created this world to reveal what is veiled. Also, the **Prophet Muhammad (Peace Be Upon Him)** who is a guidance in every aspect of life for the betterment of Humanity.

I would like to say a big thanks to my supervisor **Dr. Shafqat Hussain**, Associate Professor in Capital University of Science and Technology, for not only letting my mind to explore this problem but also helping me throughout the research and compilation of my dissertation. He has been available and ready to solve my queries at every possible time, in every possible situation, and in every possible way. His guidance and attention are an asset for me which can not be neglected and I feel honoured and blessed to work under his supervision. I am also very thankful to my teachers; **Dr. Muhammad Sagheer**; Professor in Capital University of Science and Technology; **Dr. Muhammad Afzal** Assistant professor and **Dr. Abdul Rehman Kashif**; Associate professors in capital University of science and Technology; for being a good mentor.

I would also like to mention **Ms. Ayesha Majeed** for keeping me motivated and encouraged throughout my work. I should not only thanks to her for helping me but also for tolerating my arguing nature. Her unlimited help and friendly behaviour cannot be pretermitted.

I would really like to express my gratitude to **Bilal Ahmed** and **Maleha Atlas** and my friend **Sumbal Shahid** for being a part of this work. Countless prayers of my Mother are a huge help of mine. A person who can not be ignored is my Father who let me reach at this level to believe in myself. My brothers **Fahad** and **Fakher** are also a help to me and the accomplishment of this thesis would not be possible without them. I would like to say thanks to every person again for their selfless support, devotion, care,and moral support. May ALLAH bless them all.

RukhshandaTariq

Abstract

This investigation is undertaken to explore the impact of non-linear thermal radiation on the development of Magnetohydrodynamic mixed convective, laminar, steady flow inside an enclosure having a square cylinder. The working fluid is a mixture of aluminum oxide nanoparticles and water, referred as nanofluid. As thermal boundary conditions of the cavity, two verticals surfaces are adiabatic whereas two horizontal walls are kept at different temperature T_h and T_c. The upper surface carry low temperature (T_c) and is moving with constant speed, the bottom wall is maintained at high temperature (T_h), and the central square cylinder is fixed at average temperature. The non-dimensional governing equations are simulated with the help of finite element method based on the Galerkin weighted residual technique. In particular, the biquadratic finite element space is utilized for velocity, temperature approximations while discontinuous linear element is employed for the pressure component. Picard iteration technique is implemented to linearize the discretized non-linear system of equations and then Gaussian elimination method is adopted to solve the associated linear subproblem. The computational study is demonstrated and analyzed by means of isotherms, streamlines, and some useful plots.

Contents

List of Figures

List of Tables

Abbreviations

PDEs	Partial differential equations
FEM	Finite element method
GFEM	Galerkin finite element method
FVM	Finite volume method

Symbols

C_p	specific heat constant $(Jkg^{-1}K^{-1})$
g	gravitational acceleration (ms^{-2})
k	thermal conductivity $(kgms^3K^{-1})$
$\dot{Q}$	rate of heat transfer
A	cross-sectional area normal to direction of heat flow
dT/dx	temperature gradient of the section
k^*	mean absorption coefficient
$\widetilde{L}$	length of the square cavity (m)
U_L	velocity of lid
Nu	local Nusselt number
Nu_{avg}	averaged Nusselt number
p	dimensional pressure
P	non-dimensional pressure
q_x	radiative heat flux along $x-$direction (W/m^2)
q_y	radiative heat flux along $y-$direction (W/m^2)
Pr	Prandtl number $(\frac{\nu_f}{\alpha_f})$
Ri	Richardson number $(\frac{GR}{Re^2})$
Ha	Hartmann number $(B_0\widetilde{L}\sqrt{\sigma_f/\mu_{nf}})$
Ec	Eckert number $\left(\frac{U_L^2}{C_p(T_h-T_c)}\right)$
Re	Reynolds number $(\frac{\widetilde{L}U_L}{\nu_L})$
Gr	Grashof number, $(\beta\ g\ \Delta T\ L^3/\nu^2)$
N_r	temperature ratio $(\frac{T_h}{T_c})$
Rd	thermal radiation parameter $(\frac{4\sigma^* T_c^3}{k^* k_f})$

T	fluid temperature (K)
T_h	hot lower wall temperature (K)
T_c	cold upper moving wall temperature (K)
ΔT	temperature difference (K)
T_s	surface temperature (K)
T_∞	is bulk temperature (K)
u	dimensional velocity in x-direction (ms^{-1})
U	dimensionless velocity component in x-direction
v	dimensional velocity in y-direction (ms^{-1})
V	dimensionless velocity component in y-direction
(x, y)	dimensional space coordinates (m)
(X, Y)	dimensionless space coordinates

Greek symbols

α	thermal diffusivity (m^2s^{-1})
β	thermal expansion coefficient (K^{-1})
ϕ	volume fraction of nanoparticles
θ	non-dimensional temperature $\left(\frac{T-T_c}{T_h-T_c}\right)$
ρ	density (kgm^{-3})
σ	electrical conductivity
μ	dynamic viscosity $(kgm^{-1}s^{-1})$
ν	kinematic viscosity (m^2s^{-1})
σ^*	Stefan-Boltzman constant (KW/m^2k^4)
ΔT	temperature gradient (K)

Subscripts

avg	average
c	cold
h	hot
f	fluid
nf	nanofluid
s	nanoparticles

Chapter 1

Introduction

Heat transfer is the process in which energy transfers from one place (or system) to another place due to the temperature differences of both places (or systems). Phenomena of heat transfer is classified into three groups i.e., conduction, convection and radiation. In the literature review, it has been observed that energy transfer in the base fluid through convection is acquiring the center of attraction of many researchers due to its wide applications in various engineering processes [13, 21, 33]. Convection is further classified into three sub-groups; Free or natural convection (occurs because of temperature difference which cause variation in densities), forced convection (motion of fluid is created artificially) and mixed convection (occurs due to both buoyancy and shear forces collectively play their role).

1.1 Mixed Convection in an Enclosure

The latest technology impact have intensified interest on the mixed convection flows in the cavities with the purpose of quantitative understanding of engineering applications. From the last few decades mixed convection flows in the driven enclosure is under consideration due to its applications like heat transfer in solar ponds [13], float glass production [33], etc. For the simulation of Navier-Stokes

problem driven enclosure phenomena have been widely used as a benchmark case. [41].

Computational study of influence of fixed length of heaters on combined convection in an enclosure having porous media has been investigated by Öztop [29]. Results showed that the position of heaters is very important in the heat transport and temperature gradient. Amiri *et al.* [4] numerically analyzed the combined impact of thermal and mass transport in a driven enclosure. The computational study was conducted for pertinent non-dimensional parameters with various ranges for example, Lewis number, $1 \leq Le \leq 50$, Richardson number, $4 \times 10^{-4} \leq Ri \leq 10$ and buoyancy ratio parameter, $-100 \leq N \leq 100$ to examine the mass and heat transport mechanism. Combined convection in a rectangular cavity with continuously moving horizontal plate has been discussed by Waheed [42]. Simulations of heat transport phenomena through combined convection in an enclosure with numerous values of Ri and Pr have been performed by Cheng [15]. Saha *et al.* [36] have simulated the combined convection in a driven enclosure with a wavy lower surface. Set of governing equations of physical problem has been solved with the help of GFEM. Baker *et al.* [7] have studied the combined convection in an enclosure coupled with internal heat generation. It was noticed that rate of heat transfer rate reduced by adding the heat generation.

1.1.1 Impact of Nanofluid on the Mixed Convection Flows

Mixed convection of nanofluids confined in the different geometries have gained the attention of many researchers. Fluid like engine oil, water and ethylene glycol have shown the poor properties for the heat transport. For the enhancement of the heat transfer characteristics of such fluids, researchers used micro and macro solid particles ([43]) with the base fluid (water, engine oil and ethylene glycol) by enhancing the heat conductivity of the base fluid. The suspension of metallic nanoparticles in the base fluid has been classified as a recent class of heat transfer fluids. Choi [16] initially used the nanoparticles of high thermal conductivity in

the base fluid to enhance the heat transport phenomena. Literature review revealed that the mixed convection in lid-driven enclosures poured with nanofluid has great significance among the researchers due to its various practical applications like lubrication technologies [21], chemical processing equipment [31], etc.

The numerical simulation for the combined convection in a tilted square enclosure poured with nanofluid whose upper wall was moving with constant speed have been analyzed by Abu-Nada and Chamkha [1]. It has been illustrated that the inclination angle and volume fraction of nanoparticles have the great impact on the flow field and heat transport. Arani *et al.* [5] performed the numerical simulation for the mixed convection in an enclosure filled with copper nanofluid with sinusoidal heating on vertical surfaces. This work explained that for different values of Ri clockwise vortex was generated in an enclosure while enhancing of the volume fraction of copper nanoparticles have positive impact on heat transfer. Analysis on laminar two-dimensional effect of combined convection in an enclosure using nanofluid with moving wall has been performed by Zeghbid and Bessaih [44]. Ahmed *et al.* [3] discussed the mixed convection in a cavity with double moving surfaces and filled with of micropolar nanofluid under the influence of discrete heat source.

1.1.2 MHD Effect on the Mixed Convection Flows

Magnetohydrodynamics (MHD) deals with the impact of magnetic field and heat transport in fluid flow. MHD mixed convection has been the subject of many authors due to its widespread applications such as electromagnetic casting, using liquid-metals for cooling of the nuclear reactor and plasma casting [26, 32]. Combined convection under the effect of magnetic field with various thermal and flow boundary conditions in the different geometries has been discussed in the literature.

Öztop *et al.* [30] analyzed the mixed convection flow in an enclosure with corner heaters under the impact of magnetic field using FVM. Bansal and Chatterjee [9]

have discussed the impact of magneto-convective on the heat transport phenomena in a vertical cavity poured with nanofluid and having rotating circular cylinder. Recently [6, 14, 17, 19] illustrated mixed convection in an enclosure under the influence of magnetic field. Bakar *et al.* [6] have extensively studied the MHD combined convection in a square enclosure. This work reveled that the convective flow become weaker by enhancing the magnetic field strength. combined convection in an enclosure poured with ferrofluid and having horizontal porous layer in the presence of inclined magnetic field was explored numerically by Gibanv *et al.* [17]. Numerical study of effect of inclined magnetic field on mixed convection in an enclosure together with volumetric heat generation performed by Hussain *et al.* [19] and GFEM has been used for the numerical simulation.

1.1.3 Flow around the Obstacle with the Mixed Convection

From the literature review, it has been noticed that the numerous studies based on combined convection in cavities have been taken into account for different types of geometries and boundary conditions. Mixed convection in an enclosure having internal blockages of various shapes getting the noteworthy attention of scientists and researcher from the recent years due to its frequently encountered applications [20]. Rahman *et al.* [34] performed the numerical simulation of the steady mixed convective flow in a cavity having circular cylinder in the presence of magnetic field and Joule heating. Two-dimensional laminar combined convection in a driven enclosure having a hollow circular obstacle numerically investigated by Billah *et al.* [10] for several values of the governing parameters. Results showed that the flow and heat transfer can be controlled by the hollow circular cylinder. Numerical simulation on combined convection in an enclosure having hot square cylinder have been conducted by Islam *et al.* [20] with various position of internal blockage.

Bansal and Chatterjee [9] investigated the influence of heated revolving circular obstacle in their study and results found that the direction of rotating cylinder

has no significant change on thermal parameters and fluid flow. The computational study on combined convection in an enclosure with upper moveable surface and having three hot triangular cylinders have been done by Boulahia *et al.* [11]. Maximum heat transfer was noticed when triangular blocks were arranged vertically at the left side of cavity. Addini and Nassab [2] also elaborated the effect of heated square cylinder in their research. Karbasifar *et al.* [24] performed the computational study on the mixed convection in a tilted driven enclosure with hot elliptical cylinder.

1.1.4 Impact of Non-Linear Thermal Radiation on the Mixed Convection

Thermal radiations is important in the implementation of an innovative energy system and carry a lot of significance. The emerging radiations from the hot surfaces and working fluid lead to the production of thermal radiation in inter-state of the system. Literature review revealed that the thermal radiation has great importance in high temperature and space technology applications [40]. It provides significant role in controlling polymer processing industry by using heat transfer process [38].

Addini and Nassab [2] have extensively studied on the of mixed convection and radiation effects on heat transport phenomena in an enclosure having hot square block. FVM was adopted for the numerical simulation of the governing equations. Mehmood *et al.* [28] performed the computational study on MHD combined convection in an enclosure poured with nanofluid and having porosity coupled with non-linear thermal radiation and their conclusion showed that the higher stream function value has been noticed with an increment of non-linear thermal radiations. Mixed convection in an enclosure having an inside inclined heater together with thermal radiation have been investigated by Hamici and Sadaoui [18].

1.2 Thesis Contribution

The main purpose of the present work is to explore the mixed convection in a square enclosure having uniformly heated square cylinder poured with alumina-water nanofluid coupled with the non-linear thermal radiations under the impact of magnetic field. The set of dimensionless governing equations have been solved by using GFEM. In particular bi-quadratic element (Q_2) and ${P_1}^{disc}$(linear element) are used for velocity, temperature, and pressure components respectively. Impact of the pertinent non-dimensional parameters were discussed with the help of streamlines, isotherms, and graphs.

1.3 Thesis Outline

This thesis is composed of following chapters:

Chapter 2 demonstrates some important definitions, basic governing laws and provides the overview of the solution methodology which will be used to analyze the modeled problem.

Chapter 3 provides the details of numerical analysis of research paper of Mehmood *et al.* [27] in which investigations have been carried out for the steady, MHD mixed convection flow having square blockage. GFEM has been adopted for the non-linear PDEs. Results are compiled through graphs, isotherms, and streamlines.

Chapter 4 extends the work of Mehmood *et al.* [27] for the influence of non-linear thermal radiations. The set of governing PDEs is discretized with Q_2/P_1^{disc} element. Numerical results are discussed for various physical parameters such as Ri, Ha, Rd, Nr and also their effect is illustrated by MATLAB graphs, isotherms and streamlines.

Chapter 5 summarizes the overall analysis performed in this thesis and suggests few directions for the further scope of this thesis.

Chapter 2

Fundamental Concepts and Basic Equations of Flow

In this chapter we discuss the laws, definitions relating to the fluid dynamics [8, 35] and dimensionless parameters [25]. Moreover, the methodology (FEM [23]) used for the numerical simulation of given problem is compiled along with a toy problem.

2.1 Important Definitions

Definition 2.1.1. (**Fluid**)
"A fluid is a substance that deforms continuously under the application of a shear (tangential) stress no matter how small the shear stress may be." Fluid comprises of the states of matter and include gases, liquids and plasma.

Definition 2.1.2. (**Fluid Mechanics**)
"Fluid mechanics is defined as the science that deals with the behavior of fluids at rest or in the motion, and the interaction of fluids with solids or other fluids at the boundaries."
It is further divided into two branches;

- **Fluid Dynamics**
- **Fluid Statics**

Definition 2.1.3. (**Fluid Dynamics**)

"The study of fluids in motion, where pressure forces are also considered that branch of science is called fluid dynamics."

Newton's second law of motion for accelerating bodies is used to represent the equation of fluid dynamics,

$$\sum \mathbf{F} = m\mathbf{a}$$

Definition 2.1.4. (**Fluid Statics**)

"Fluid statics deals with problems associated with fluids at rest. Fluid statics is generally referred to as hydrostatics when the fluid is a liquid and as aerostatics when the fluid is a gas."

Newton's second law for non-accelerating bodies is used to describe the basic equation of fluid statics, i.e

$$\sum \mathbf{F} = 0$$

Definition 2.1.5. (**Viscosity**)

"Viscosity is defined as the property of a fluid which offers resistance to the movement of one layer of fluid over another adjacent layer of the fluid."

Definition 2.1.6. (**Kinematic Viscosity**)

"It is the ratio between the dynamic viscosity and density of fluid."

$$\nu = \frac{\mu}{\rho}$$

Definition 2.1.7. (**Nanofluid**)

"Nanofluids are engineered colloids made of a base fluid and nanoparticles $(1-100)$ nm. Nanofluids have higher thermal conductivity and single-phase heat transfer coefficients than their base fluids [12]." Metals, oxides, carbides, or carbon nanotubes are the typical nanoparticles which are used in nanofluids and oil, ethylene glycol and water are the examples of common base fluids.

2.2 Classification of Fluids

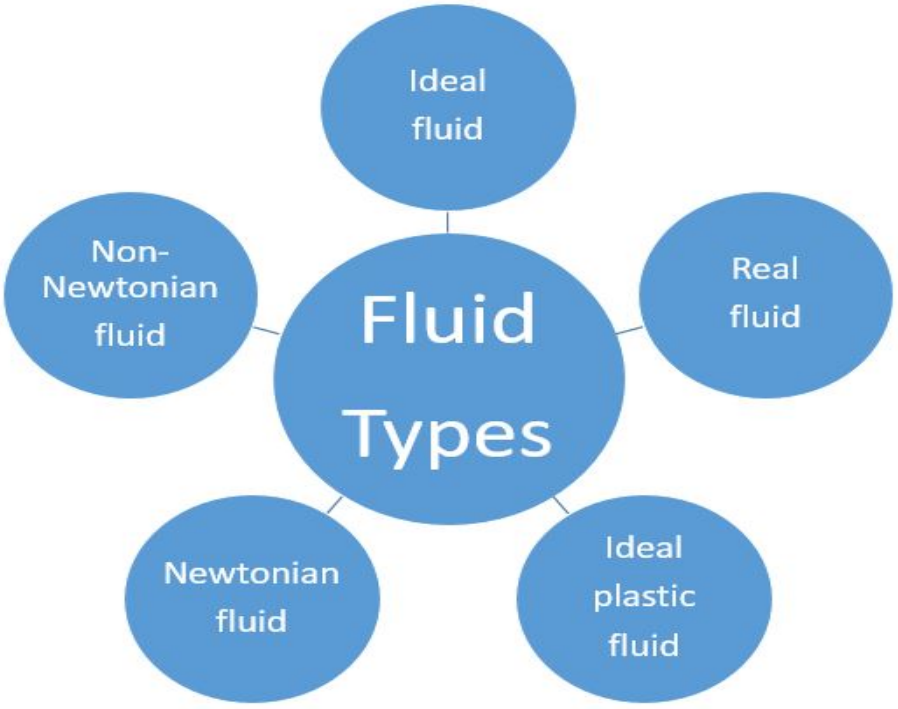

Definition 2.2.1. (**Ideal Fluid vs Real Fluid**)
"A fluid which is incompressible and is having no viscosity, is known an ideal fluid." Practically no ideal fluid exists. Whereas, "A fluid, which possess viscosity, is known as real fluid." Real fluids are compressible.

Definition 2.2.2. (**Ideal plastic fluid**)
"A fluid, in which shear stress is more than the yield value and shear stress is proportional to the rate of shear strain (or velocity gradient), is known as ideal plastic fluid. Printers ink and other thixotropic substance are the examples of real plastic fluids."

Definition 2.2.3. (**Newtonian Fluid vs non-Newtonian Fluid**)
"A real fluid, in which the shear stress is directly, proportional to the rate of shear strain (or velocity gradient), is known as a Newtonian fluid." In Newtonian fluids, water, light-hydrocarbon oils, Benzine , Silicone oil etc are comes. On the other hand, "A real fluid, in which the shear stress is not proportional to the rate of

shear strain (or velocity gradient), is known as a Non-Newtonian fluid." Slurries, Pastes, Plaster etc are considered as non-Newtonian fluid.

2.3 Flow and its Types

Flow is relating to the movement of material. The fluid flow is classified as

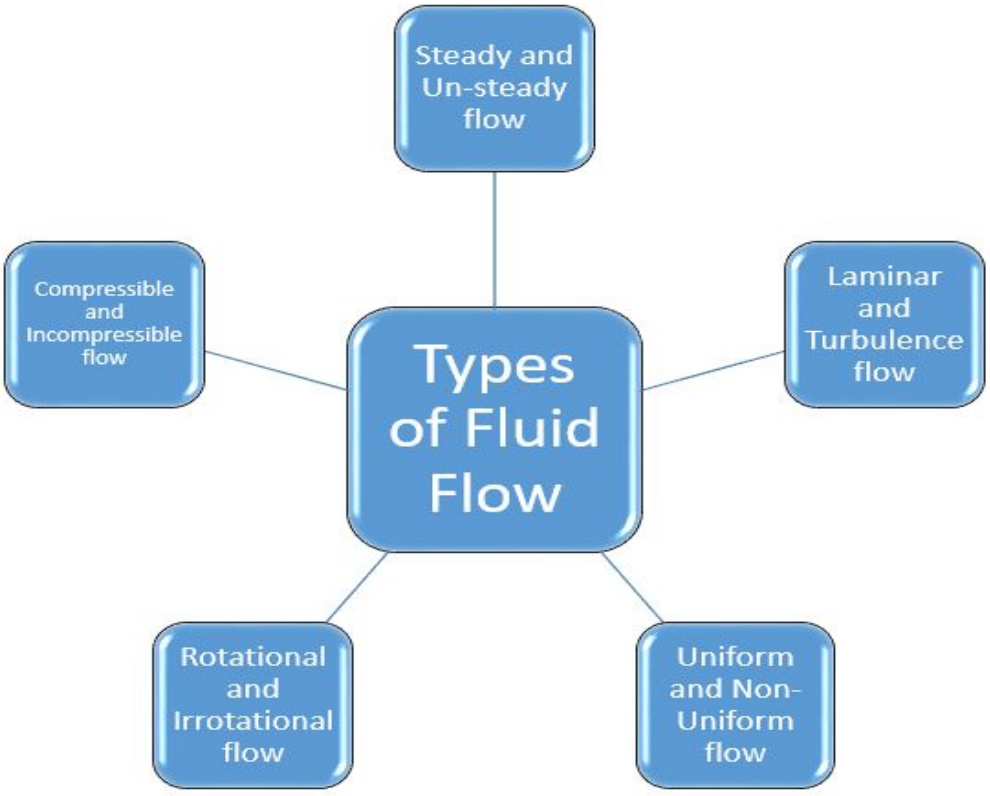

Definition 2.3.1. (**Steady vs Unsteady Flow**)
"Steady flow is defined as that type of flow in which the fluid characteristics like velocity, pressure, density, etc. at a point do not change with time." Mathematically representation of steady flows is,

$$\frac{\partial P^*}{\partial t} = 0$$

On the other side, "Unsteady flow is that type of flow, in which the velocity, pressure and density at a point changes with respect to time." Thus, mathematically

it is written as

$$\frac{\partial P^*}{\partial t} \neq 0$$

here any property like pressure, velocity or density are represented by P^*.

Definition 2.3.2. (**Uniform flow vs non-Uniform Flows**)
"Uniform flow is defined as, a flow in which the velocity at any given time does not change with respect to space (i.e., length of direction of the flow)." Mathematical expression for uniform flow

$$\left(\frac{\partial \mathbf{V}}{\partial s}\right)_{t=constant} = 0$$

"Non-uniform flow is that type of flow in which the velocity at any given time change with respect to space." It is written as

$$\left(\frac{\partial \mathbf{V}}{\partial s}\right)_{t=constant} \neq 0$$

change of velocity and length of flow in direction s are represented by $\partial \mathbf{V}$ and ∂s respectively.

Definition 2.3.3. (**Laminar vs Turbulent Flow**)
"Laminar flow is defined as, in which the fluid particles move along well-defined paths or stream line and all the stream lines are straight and parallel. Thus the particles move in laminas or layer gliding smoothly over the adjacent layer." Whereas,
"Turbulent flow is that type of flow in which the fluid particles move in a zig-zag way. Due to the movement of fluid particles in a zig-zag way, the eddies formation takes place which are responsible for high energy loss."

Definition 2.3.4. (**Compressible vs Incompressible Flow**)
"The flow in which the density of the fluid changes from point or in other words the density (ρ) is not constant for the fluid."

$$\rho \neq constant$$

"An incompressible flow, in which the density is constant for the fluid flow."

$$\rho = constant$$

2.4 Modes of Heat Transfer and Related Properties

Definition 2.4.1. (**Heat**)
In thermodynamics, "Heat is defined as the form of energy that is transferred across the boundary of a system at a given temperature to another system (or the surroundings) at a lower temperature by virtue of the temperature difference between the two systems."

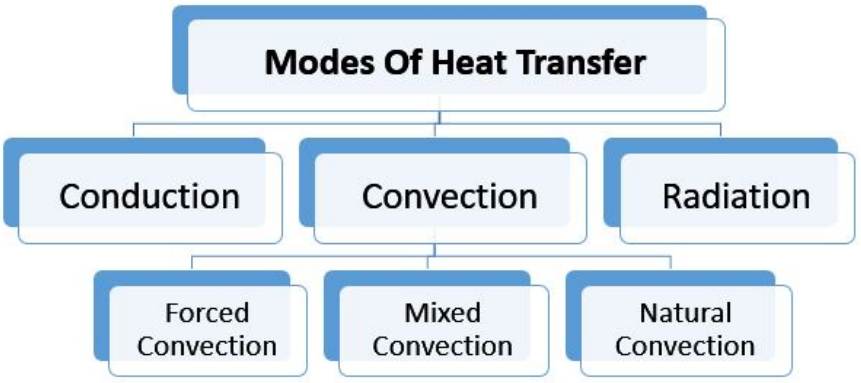

Definition 2.4.2. (**Conduction**)
"Conduction is the transfer of heat from one body at a higher temperature to another body in physical contact with it at a lower temperature. The conduction process takes place at the molecular level and involves the transfer of energy from the more energetic molecules to those with a lower energy level."
Mathematical expression for conduction phenomena.

$$\dot{Q} = -kA(dT/dx).$$

Definition 2.4.3. (**Convection**)

"Convection, relates to the transfer of heat from a bounding surface to a fluid in motion, or to the heat transfer across a flow plane within the interior of the flowing fluid." Mathematically convection can be written as,

$$\dot{Q} = hA(T_s - T_\infty).$$

Natural Convection

"If the fluid motion occurs as a result of the density difference produced by the temperature difference, the process is called free or natural convection."

Forced Convection

"If the fluid motion is induced by a pump, a blower, a fan, or some similar device, the process is called forced convection."

Mixed Convection

"When heat transfer occurs due to the combination of free convection and forced convection is known as mixed convection." Nuclear technology and some aspects of electronic cooling is the example of mixed convection.

Definition 2.4.4. (**Radiation**)

"Radiation, or more correctly thermal radiation, is electromagnetic radiation emitted by a body by virtue of its temperature and at the expense of its internal energy. Medium is not necessary for heat transfer through radiation."

Definition 2.4.5. (**Joule Heating**)

"Joule heating is the energy dissipation that occurs with an electric current flowing through a resistor."

Definition 2.4.6. (**Thermal Diffusivity**)

"It measures the ability of material to conduct thermal energy relative to its ability to store thermal energy means how fast or how easily heat can penetrate an object or substance." It's mathematical form is

$$\alpha = \frac{k}{\rho C_p}.$$

Definition 2.4.7. (**Thermal Conductivity**)

"Under the heat transfer conditions, the effectiveness with which a material conduct heat is considered as a thermal conductivity." In the case of solid, free electrons are responsible for the thermal conductivity of material, for liquid and gases it is due to lattice vibrational wave. Thermal conductivity of pure metals are higher than the other materials.

2.5 Dimensionless Parameters

Definition 2.5.1. (**Hartmann Number**)

Hartmann number first introduced by Hartmann and defined as,

" The ratio of the induced electrodynamic (magnetic) force to the hydrodynamic force of the viscosity."

It is a dimensionless number used in Plasma. It's mathematical form is

$$Ha = B_0 \widetilde{L} \sqrt{\frac{\sigma}{\mu}}$$

Definition 2.5.2. (**Prandtl Number**)

"This number expresses as the ratio of the momentum diffusivity (viscosity) to the thermal diffusivity."

German physicist, Ludwig Prandtl first gave the idea of this number and can be expressed as,

$$Pr = \frac{\nu}{\alpha}$$

Definition 2.5.3. (**Reynolds Number**)

The physical interpretation of Reynolds number is,

"The ratio of the fluid inertia force to that of molecular friction (viscosity)."

Mathematically it can be written as,

$$Re = \frac{\rho \mathbf{V} \widetilde{L}}{\mu} = \frac{\mathbf{V} \widetilde{L}}{\nu}$$

where, $\mathbf{V}$ represents the velocity of fluid.

Definition 2.5.4. (**Eckert Number**)

"It expresses the ratio of kinetic energy to a thermal energy change."

It named after Ernst R.G Eckert in the early 1950s, it can be expressed as,

$$Ec = \frac{\mathbf{V}^2}{C_p(T_h - T_c)}$$

Definition 2.5.5. (**Grashof Number**)

Another dimensionless parameter is Grashof which defined as,

"It expresses the buoyancy-to-viscous forces ratio and its action on a fluid. It characterizes the free non-isothermal convection of the fluid due to the density difference caused by the temperature gradient in the fluid."

German engineer Franz Grashof introduced this number and mathematically,

$$Gr = \frac{g\beta(T_h - T_c)\widetilde{L^3}}{\nu}$$

here, velocity is represented by $\mathbf{V}$.

Definition 2.5.6. (**Richardson Number**)

Richardson number is a non-dimensional parameter named after Lwis Fry Richardson $(1881 - 1953)$, Ri defined as, "It is the ratio of the buoyancy term to the flow shear term." It's mathematical form is

$$Ri = \frac{g\nabla\rho}{\rho(\nabla\mathbf{V})^2}$$

$\mathbf{V}$ is velocity of fluid. Ri also expressed as the combination of Grashof number to Reynolds number.

$$Ri = \frac{Gr}{Re^2}$$

Definition 2.5.7. (**Nusselt Number**)

"It expresses the ratio of the total heat transfer in a system to the heat transfer by conduction." Mathematically,

$$Nu = \frac{\widetilde{Q}_{conv}}{\widetilde{Q}_{cond}} = \frac{h\Delta T}{k\frac{\Delta T}{L}} = \frac{hL}{k}$$

If, $Nu \gg 1$, more effective heat transfer through convection. $Nu = 1$, fluid is stationary and all the heat transfer is by conduction.

2.6 Fundamental Equations of Flow

Definition 2.6.1. (**Continuity Equation**)
"The conservation of mass of fluid entering and leaving the control volume, the resulting mass balance is called the equation of continuity." This equation reflects the fact that mass is conserved. Mathematically it can be write as

$$\frac{\partial \rho}{\partial t} + \nabla .\ (\rho\ \mathbf{V}) = 0.$$

where, $\mathbf{V}$ is velocity of fluid.

For steady case rate of time will be constant, so continuity equation becomes

$$\nabla .\ (\rho\ \mathbf{V}) = 0.$$

In the case of incompressible flow, density does not variate so continuity equation can be re-write as,

$$\nabla .\ \mathbf{V} = 0.$$

Definition 2.6.2. (**Law of Conservation of Momentum**)
It is based on the momentum principle, which states that,
"The net force acting on a fluid mass is equal to the change in momentum of flow per unit time in that direction." Mathematically this law can be written as

$$\rho \frac{D\mathbf{V}}{Dt} = \rho\ \mathbf{f} + \nabla .\ \underline{T}, \tag{2.1}$$

For Navier-Stokes equation

$$\underline{\mathrm{T}} = -pI + \tau, \tag{2.2}$$

where τ is a tensor and it can be written as,

$$\tau = \mu \left(\nabla \mathbf{V} + (\nabla \mathbf{V})^{t^*} \right), \tag{2.3}$$

In the above equations, $\frac{D}{Dt}$ denotes material time derivative or total derivative, ρ denotes density, $\mathbf{V}$ denotes velocity of fluid, Cauchy stress tensor represented by τ, $\mathbf{f}$ is the body forces, p is the pressure and t^* is transpose of matrix. Matrix form of Cauchy stress tensor is

$$\tau = \begin{pmatrix} \sigma_{xx} & \tau_{xy} & \tau_{xz} \\ \tau_{xy} & \sigma_{yy} & \tau_{yz} \\ \tau_{zx} & \tau_{zy} & \sigma_{zz} \end{pmatrix}, \tag{2.4}$$

For two-dimensional flow, we have $\mathbf{V} = [u(x, y, 0),\ v(x, y, 0),\ 0]$ and thus

$$\nabla \mathbf{V} = \begin{pmatrix} \frac{\partial u}{\partial x} & \frac{\partial v}{\partial x} & 0 \\ \frac{\partial u}{\partial y} & \frac{\partial v}{\partial y} & 0 \\ 0 & 0 & 0 \end{pmatrix}, \tag{2.5}$$

$$(\nabla \mathbf{V})^{t^*} = \begin{pmatrix} \frac{\partial u}{\partial x} & \frac{\partial u}{\partial y} & 0 \\ \frac{\partial v}{\partial x} & \frac{\partial v}{\partial y} & 0 \\ 0 & 0 & 0 \end{pmatrix}, \tag{2.6}$$

Substituting Eqs. (2.5) and (2.6) into Eq. (2.3) and then in Eq. (2.2) it is found that:

$$T_{xx} = -p + 2\mu \frac{\partial \mu}{\partial x} \tag{2.7}$$

$$T_{xy} = \mu \left(\frac{\partial \nu}{\partial x} + \frac{\partial u}{\partial y} \right) \tag{2.8}$$

Using Eqs. (2.7) to (2.8) in Eq. (2.1), we get two-dimensional Naiver-Stokes equation for u component.

$$\rho \frac{Du}{Dt} = \rho \underline{f}_x - \frac{\partial p}{\partial x} + \mu \left(\frac{\partial^2 u}{\partial x^2} + \frac{\partial^2 u}{\partial y^2} \right) \tag{2.9}$$

Similarly, by repeating the above process for v component, we get

$$\rho\frac{Dv}{Dt} = \rho\underline{f}_y - \frac{\partial p}{\partial y} + \mu\left(\frac{\partial^2 v}{\partial x^2} + \frac{\partial^2 v}{\partial y^2}\right) \tag{2.10}$$

Definition 2.6.3. (**Law of Conservation of Energy**)
The basic principle of conservation of energy is that, "Energy can neither created nor destroyed, it can be transformed from one form to another form but total amount of an isolated system remains constant i.e. energy is conserved over time." It is the fundamental law of physics which is also referred to as the first law of thermodynamics.

The energy equation in two-dimensional for pure fluid can be written as,

$$\left(u\frac{\partial T}{\partial x} + v\frac{\partial T}{\partial y}\right) = \alpha\left(\frac{\partial^2 T}{\partial x^2} + \frac{\partial^2 T}{\partial y^2}\right) + \frac{\mu}{\rho C_p}\widetilde{\Phi} \tag{2.11}$$

where $\widetilde{\Phi}$ is dissipation function.

2.7 Finite Element Method

The partial differential equations (PDEs) describe those problems which depend on more then one variables like, space and time dependent problems. Most of those PDEs can not be solved with analytical approach. Therefore, different discretization methods based approximation can be constructed to tackle such equations. One of the method for such approximations is"Finite element method", which was first discussed by Clough in 1960. In the early $1960s$, engineers used the method for the approximate solutions of problems in stress analysis, heat transfer, fluid flow, electromagnetic potential, structural analysis, and mass transport. The analytical solution of these problems generally requires the solution to boundary value problems for partial differential equations. The finite element method formulation of the problem results in a system of algebraic equations. The method yields approximate values of the unknowns at the discrete number of points over the domain.

2.7.1 Galerkin Weighted Residual Technique

In numerical analysis technique, Galerkin methods considered as a class of methods which are used to convert a continuous operator problem (such as PDEs) to a discrete problems. Main objective of this method is to achieve the weak formulation which is equivalent to the method of variation of parameters to a function space. In the Galerkin method of weighted residuals, the most common method is FEM, which is used to calculating the global stiffness matrix. The main features of FEM are listed below.

1. **Construct a Variational/Weak Formulation**

   - To achieve the variational form of the given strong form first step is multiply the differential equation with suitable weight (test) function $\widetilde{w}$ which satisfy the homogenous boundary conditions for the Dirichlet boundary and then perform the integrate over the whole domain (using integration by parts or Green's theorem)
   - Enforce the Neumann boundary conditions on the boundary integrals and Dirichlet boundary conditions on the trial function.

2. **Formulate a Mesh and Basis Function**

   - For one-dimensional domain [a,b], a mesh is a set of points in the interval of interest. say, $x_0 = a, x_1, x_2, ..., x_M = b$. Let $h_i = x_{i+1} - x_i, i = 0, 1, 2, ..., M - 1$.
   - x_i is called the nodal point or node.
   - (x_i, x_{i+1}) is called an element.
   - $h = \max\limits_{0 \leq i \leq i+1} h_i$ is the mesh size.
   - Approximate the infinite dimensional trial and test spaces U and W by the finite dimensional spaces U_h and W_h respectively.
     U_h (finite dimensional spaces) $\subset U$ (the solution space).

- Since U_h has a finite dimension, we can find a set of basis functions, $\varepsilon_1, \varepsilon_2, \varepsilon_3, ..., \varepsilon_{M-1} \subset U_h$ that are linearly independent, i.e.

$$u_h \approx \sum_{j=1}^{M-1} a_j \varepsilon_j \subset U_h$$

where, ε_j is a basis function and a_j are the unknown solution values at the nodes

3. **Linear System**

- Computing the linear system of equations for the coefficients a_j results in approximate solution

$$u_h \approx \sum_{j=1}^{M-1} a_j \varepsilon_j$$

For the demonstration of Galerkin weighted residual formulation, the following example is considered.

Example

Consider a 2D, steady poisson equation.

$$-\Delta T = f, \quad \text{in} \quad \Omega \tag{2.12}$$

$$T = 0, \quad \text{on} \quad \partial\Omega \tag{2.13}$$

here f is known function and T is to be found, Ω is domain of the problem which is open, bounded, and connected and $\partial\Omega$ is the boundary.

- The exact solution T of the Eq. (2.12) should be twice continuously differentiable and satisfying Eq. (2.12). Let $\widetilde{w}$ be a weight (test) function such that $\widetilde{w}(x, y) = 0$ on the boundary of the domain.

- To attain the weak formulation, weighted residual integral statement of the Eq. (2.12) is

$$-\int_\Omega \widetilde{w}\ \Delta T d\Omega = \int_\Omega \widetilde{w} f d\Omega, \tag{2.14}$$

- Green's theorem is used to get the first order derivatives from second order derivatives.

$$\int_{\Omega} \widetilde{w}\ \frac{\partial T}{\partial n} ds = \int_{\Omega} \nabla \widetilde{w}\ \nabla T d\Omega + \int_{\Omega} \widetilde{w}\ \Delta T d\Omega \tag{2.15}$$

- Substitute Eq. (2.15) into Eq. (2.14), we gets

$$\underbrace{-\int_{\Omega} \frac{\partial T}{\partial n} ds}_{0} + \int_{\Omega} \nabla \widetilde{w}\ \nabla T d\Omega = \int_{\Omega} \widetilde{w} f d\Omega, \tag{2.16}$$

  homogeneous boundary conditions result in canceling the boundary integral, so we obtained as

$$\int_{\Omega} \nabla \widetilde{w}\ \nabla T d\Omega = \int_{\Omega} \widetilde{w} f d\Omega, \tag{2.17}$$

- Elemental weak form is

$$\int_{\Omega_e} \nabla \widetilde{w}\ \nabla T d\Omega = \int_{\Omega^e} \widetilde{w} f d\Omega, \tag{2.18}$$

- In cartesian (2D) plane, Eq. (2.18) may be written as

$$\int_{\Omega^e} \left(\frac{\partial \widetilde{w}}{\partial x} \frac{\partial T}{\partial x} + \frac{\partial \widetilde{w}}{\partial y} \frac{\partial T}{\partial y} \right) d\Omega = \int_{\Omega^e} \widetilde{w} f d\Omega, \tag{2.19}$$

- Approximate the solution over an element as

$$T^e = \sum_{j=1}^{M} T^e{}_j\ \varepsilon^e{}_j(x, y) \tag{2.20}$$

  where ε_j is a basis function and T_j are the solution values at nodes.

- Substituting the approximate solution from Eq. (2.20) into the weak form (Eq. (2.19))

$$\int_{\Omega^e} \left[\left(\sum_{j=1}^{M} T^e{}_j \frac{\partial \varepsilon^e{}_j}{\partial x} \right) \frac{\partial \widetilde{w}}{\partial x} + \left(\sum_{j=1}^{M} T^e{}_j \frac{\partial \varepsilon^e{}_j}{\partial y} \right) \frac{\partial \widetilde{w}}{\partial y} \right] d\Omega = \int_{\Omega^e} \widetilde{w} f d\Omega, \tag{2.21}$$

- By using GFEM we choose a weight function, $\widetilde{w} = {\varepsilon^e}_i$ to get the following *ith* equation of elemental system

$$\int_{\Omega^e} \left[\left(\sum_{j=1}^{M} {T^e}_j \frac{\partial {\varepsilon^e}_j}{\partial x} \right) \frac{\partial {\varepsilon^e}_i}{\partial x} + \left(\sum_{j=1}^{M} {T^e}_j \frac{\partial {\varepsilon^e}_j}{\partial y} \right) \frac{\partial {\varepsilon^e}_i}{\partial y} \right] d\Omega = \int_{\Omega^e} {\varepsilon^e}_i f d\Omega, \tag{2.22}$$

$$\sum_{j=1}^{M} \underbrace{\left[\int_{\Omega^e} \left(\frac{\partial {\varepsilon^e}_j}{\partial x} \frac{\partial {\varepsilon^e}_i}{\partial x} + \frac{\partial {\varepsilon^e}_j}{\partial y} \frac{\partial {\varepsilon^e}_i}{\partial y} \right) d\Omega \right]}_{K^e} {T^e}_j = \underbrace{\int_{\Omega^e} {\varepsilon^e}_i f d\Omega}_{F^e}. \tag{2.23}$$

- The Eq. (2.23) can be written in the compact form as

$$[K^e] \{T^e\} = \{F^e\} \tag{2.24}$$

  here, $[K^e]$, $\{T^e\}$, $\{F^e\}$ represents the **elemental stiffness matrix**, **vector of elemental nodal** and **elemental force vector** respectively.

- The following global system can be obtained, when the elemental systems are assembled.

$$[K] \{T\} = \{F\} \tag{2.25}$$

Chapter 3

Simulation of MHD Mixed Convection Nanofluid Flow in a Cavity with an Obstacle

In this chapter, we are interested to investigate the mixed convection in a driven enclosure having an isothermally heated square cylinder filled with an alumina-water nanofluid under the impact of magnetic field. For this purpose, first we transform the dimensional governing equations into the non-dimensional coupled PDEs. Then these non-dimensional governing equations are discretized using the GFEM. The impact of different parameters are analyzed with the help of streamlines, isotherms and MATLAB graphs. This chapter provides the detailed review of [27].

3.1 Problem Formulation

The system to be investigated is a lid-driven square enclosure with an isothermal heated block placed in the center of the cavity. Physical situation is demonstrated by a schematic diagram of given problem as shown in Figure 3.1.

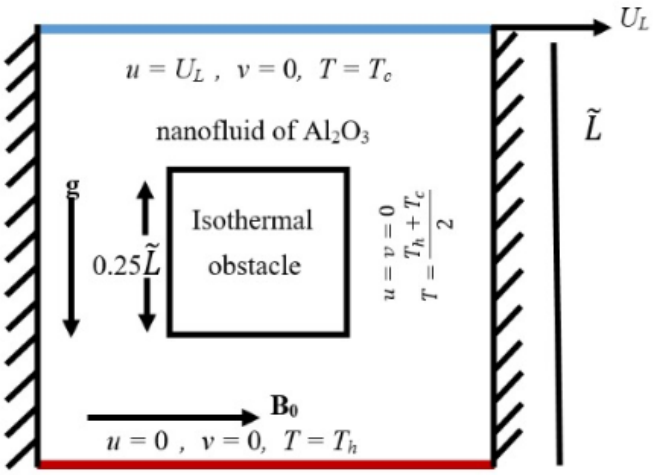

Figure 3.1: Schematic diagram of the physical problem

The length and width of the square cavity is $\widetilde{L}$ and $0.25\widetilde{L}$ is the size of central square cylinder. The upper surface of square enclosure is moving in its own plane with uniform velocity U_L while other walls of cavity are at rest. Temperature of lower and upper surfaces of the cavity are maintained as T_h and T_c where $T_h > T_c$ while the side walls are kept adiabatic. Whereas uniform average temperature $(\frac{T_h+T_c}{2})$ is maintained for the central square cylinder. A constant magnitude of magnetic field B_0 is imposed in the positive x direction perpendicular to the vertical adiabatic walls. The induced magnetic field which is produced due to the motion of electrically conducting fluid is ignored as compared to the external magnetic field. The nanofluid which is under investigation is assumed to be steady, incompressible, Newtonian and laminar. Moreover, viscous dissipation, the induced electrical fields and thermal radiation in the energy equations are ignored [6, 30], whereas Joule heating is taken into account while modeling the energy equation [34]. The gravitational acceleration is acting towards the negative y direction. Thermo-physical properties of aluminium particles are kept constant (see Table 3.1) and Boussinesq approximation has been adopted for the buoyancy term in momentum equation.

Physical Properties	H_2O	Al_2O_3
$C_p(JKg^{-1}K^{-1})$	4179	765
$k(Wm^{-1}K^{-1})$	0.613	40
$\beta(K^{-1})$	21×10^{-5}	0.85×10^{-5}
$\sigma(\Omega m^{-1})$	0.05	1×10^{-10}
$\rho(kgm^{-3})$	997.1	3970

Table 3.1: Thermophysical properties of Al_2O_3 and H_2O.

The Governing Equations

Under on the aforementioned assumptions for the proposed problem, the dimensional steady form of continuity, momentum, and energy equation together with boundary conditions are given below [27].

- Continuity Equation:

$$\frac{\partial u}{\partial x} + \frac{\partial v}{\partial y} = 0, \tag{3.1}$$

- u Momentum Equation:

$$u\frac{\partial u}{\partial x} + v\frac{\partial u}{\partial y} = -\frac{1}{\rho_{nf}}\frac{\partial p}{\partial x} + \frac{\mu_{nf}}{\rho_{nf}}\left(\frac{\partial^2 u}{\partial x^2} + \frac{\partial^2 u}{\partial y^2}\right) \tag{3.2}$$

- v Momentum Equation:

$$u\frac{\partial v}{\partial x} + v\frac{\partial v}{\partial y} = -\frac{1}{\rho_{nf}}\frac{\partial p}{\partial y} + \frac{\mu_{nf}}{\rho_{nf}}\left(\frac{\partial^2 v}{\partial x^2} + \frac{\partial^2 v}{\partial y^2}\right) + \frac{(\rho\beta)_{nf}}{\rho_{nf}} g\,(T - T_c) - \frac{\sigma_{nf} B_0^2}{\rho_{nf}} v \tag{3.3}$$

- Energy Equation:

$$u\frac{\partial T}{\partial x} + v\frac{\partial T}{\partial y} = \alpha_{nf}\left(\frac{\partial^2 T}{\partial x^2} + \frac{\partial^2 T}{\partial y^2}\right) + \frac{\sigma_{nf} B_0^2}{(\rho C_p)_{nf}} v^2 \tag{3.4}$$

Dimensional Boundary Conditions

The dimensional form of the boundary conditions on each wall of the square cavity and the inside blockage is given as:

- On the top wall:

$$u(x,y) = U_L, \quad v(x,y) = 0, \quad T = T_c$$

- On the lower wall:

$$u(x,y) = 0, \quad v(x,y) = 0, \quad T = T_h$$

- On the vertical walls:

$$u(x,y) = 0, \quad v(x,y) = 0, \quad \frac{\partial T}{\partial x} = 0$$

- On the blockage inside the cavity:

$$u(x,y) = 0, \quad v(x,y) = 0, \quad T = \frac{1}{2}.(T_h + T_c)$$

Effective Properties of Nanofluid

Properties of the nanofluid are attributed to the properties of nanoparticles and the base fluid. Various correlations have been suggested and utilized for the simulations of nanofluids in the literature. The correlations used in this thesis are given by [27]

- Effective Density:

$$\rho_{nf} = \rho_f + \phi\rho_f$$

- Thermal Diffusivity:

$$\alpha_{nf} = k_{nf}.\frac{1}{(\rho c_p)_{nf}}$$

- Electrical Conductivity:

$$\frac{\sigma_{nf}}{\sigma_f} = \left[1 + 3\left(\sigma - 1\right)\phi.\{(\sigma+2)(\sigma-1)\phi\}^{-1}\right], \quad \sigma = \frac{\sigma_s}{\sigma_f}$$

- Specific Heat:

$$(\rho C_p)_{nf} = (\phi + 1)(\rho C_p)_f + \phi(\rho C_p)_s$$

- Coefficient of Thermal Expansion:

$$(\rho\beta)_{nf} = (\phi + 1)(\rho\beta)_f + \phi(\rho\beta)_s$$

- Thermal Conductivity:

$$k_{nf} = k_f . \left[\left\{ \frac{k_s + 2k_f + 2\phi(k_f - k_s)}{k_s + 2k_f - 2\phi(k_f - k_s)} \right\}^{-1} \right]$$

- Dynamic Viscosity:

$$\mu_{nf} = \frac{\mu_f}{(1-\phi)^{2.5}}$$

Non-Dimensional Equations

With the help of following dimensionless parameters:

$$X = \frac{x}{\widetilde{L}}, \quad Y = \frac{y}{\widetilde{L}}, \quad U = \frac{u}{U_L}, \quad V = \frac{v}{U_L}, \quad \theta = \frac{T - T_c}{T_h - T_c}, \quad P = \frac{p}{\rho_{nf} {U_L}^2},$$
$$Re = \frac{U_L \widetilde{L}}{\nu_f}, \quad Gr = \frac{g\beta_f (T_h - T_c)\widetilde{L}^3}{\nu_f^2}, \quad Ha = B_0 \widetilde{L}\sqrt{\frac{\sigma_f}{\mu_f}}, \quad Pr = \frac{\nu_f}{\alpha_f},$$
$$Ri = \frac{Gr}{Re^2}, \quad Ec = \frac{{U_L}^2}{(C_p)_f (T_h - T_c)}.$$

the governing Eqs. (3.1) to (3.4) are transformed to the dimensionless equations:

$$\frac{\partial U}{\partial X} + \frac{\partial V}{\partial Y} = 0, \tag{3.5}$$

$$U\frac{\partial U}{\partial X} + V\frac{\partial U}{\partial Y} = -\frac{\partial P}{\partial X} + \frac{1}{Re}\frac{\rho_f}{\rho_{nf}}\frac{1}{(1-\phi)^{2.5}}\left(\frac{\partial^2 U}{\partial X^2} + \frac{\partial^2 U}{\partial Y^2}\right), \tag{3.6}$$

$$U\frac{\partial V}{\partial X}+V\frac{\partial V}{\partial Y}=-\frac{\partial P}{\partial Y}+\frac{1}{Re}\frac{\rho_f}{\rho_{nf}}\frac{1}{(1-\phi)^{2.5}}\left(\frac{\partial^2 V}{\partial X^2}+\frac{\partial^2 V}{\partial Y^2}\right)$$
$$+Ri\frac{\rho_f}{\rho_{nf}}\left(1-\phi+\frac{\rho_s\beta s}{\rho_f\beta_f}\phi\right)\theta-\frac{\rho_f}{\rho_{nf}}\frac{\sigma_{nf}}{\sigma_f}\frac{Ha^2}{Re}V, \tag{3.7}$$

$$U\frac{\partial \theta}{\partial X}+V\frac{\partial \theta}{\partial Y}=\frac{\alpha_{nf}}{\alpha_f}\frac{1}{RePr}\left(\frac{\partial^2 \theta}{\partial X^2}+\frac{\partial^2 \theta}{\partial Y^2}\right)+\frac{Ha^2 Ec}{Re}\frac{\sigma_{nf}}{\sigma_f}\frac{(\rho C_p)_f}{(\rho C_p)_{nf}}V^2. \tag{3.8}$$

Dimensionless Boundary Conditions

The associated boundary conditions are reduced as follows:

- On the upper surface:

$$U(X,Y)=1,\quad V(X,Y)=0,\quad \theta=0$$

- On the lower surface:

$$U(X,Y)=0,\quad V(X,Y)=0,\quad \theta=1$$

- On the vertical surfaces:

$$U(X,Y)=0,\quad V(X,Y)=0,\quad \frac{\partial \theta}{\partial X}=0$$

- On the blockage inside the cavity:

$$U(X,Y)=0,\quad V(X,Y)=0,\quad \theta=0.5$$

Physical Quantities of Interest

Apart from the flow and the temperature gradient in the enclosure, one of the basic physical quantity of interest is the local and average Nusselt number, where

Nu is determines as the ratio of rate of heat transfer of convection to conduction. Local Nu can be computed using relation given below

$$Nu = -\frac{k_{nf}}{k_f}\left(\frac{\partial\theta}{\partial Y}\right)|_{Y=0}.$$

Nu_{avg} is given by

$$Nu_{avg} = \int_0^1 Nu dx.$$

3.2 Solution Methodology

FEM is used to solve the system of coupled nonlinear partial differential Eqs. (3.5) to (3.8) along with associated boundary conditions. To achieve this task, first we establish the variational form of the governing non-dimensional equations and then approximate the solution implementing the GFEM. The main steps involved in this method are further explained.

3.2.1 Weak/Variational Formulation

Variational form of the non-dimensional governing dimensionless partial differential equations means converting them into integral form, by multiplying the equations with suitable weight function and then performing integration over the whole domain. The strong form of the governing equations can be re-written as:

$$U\frac{\partial U}{\partial X} + V\frac{\partial U}{\partial Y} = -\frac{\partial P}{\partial X} + \Delta_1\left(\frac{\partial^2 U}{\partial X^2} + \frac{\partial^2 U}{\partial Y^2}\right), \tag{3.9}$$

$$U\frac{\partial V}{\partial X} + V\frac{\partial V}{\partial Y} = -\frac{\partial P}{\partial Y} + \Delta_1\left(\frac{\partial^2 V}{\partial X^2} + \frac{\partial^2 V}{\partial Y^2}\right) + \Delta_2\theta - \Delta_3 V, \tag{3.10}$$

$$\frac{\partial U}{\partial X}+\frac{\partial V}{\partial Y}=0, \tag{3.11}$$

$$U\frac{\partial \theta}{\partial X}+V\frac{\partial \theta}{\partial Y}=\Delta_4\left(\frac{\partial^2\theta}{\partial X^2}+\frac{\partial^2\theta}{\partial Y^2}\right)+\Delta_5 V^2. \tag{3.12}$$

where Δ_i's in the above equations are given by

$$\Delta_1=\frac{1}{Re}\frac{\rho_f}{\rho_{nf}}\frac{1}{(1-\phi)^{2.5}},\quad \Delta_2=Ri\frac{\rho_f}{\rho_{nf}}\left(1-\phi+\frac{\rho_s\beta s}{\rho_f\beta_f}\phi\right),\quad \Delta_3=\frac{\rho_f}{\rho_{nf}}\frac{\sigma_{nf}}{\sigma_f}\frac{Ha^2}{Re},$$

$$\Delta_4=\frac{\alpha_{nf}}{\alpha_f}\frac{1}{RePr},\quad \Delta_5=\frac{Ha^2Ec}{Re}\frac{\sigma_{nf}}{\sigma_f}\frac{(\rho C_p)_f}{(\rho C_p)_{nf}}.$$

In order to obtain the weak or variational form, we multiply both sides of the momentum and energy equations with test function $\widetilde{w}\in\mathbf{W}$ and multiply both sides of continuity equation with test function $\widetilde{q}\in Q$, then integrate over the whole computational domain (Ω). Here $\mathbf{W}$ and Q are the test spaces, $\mathbf{W}=[H_1(\Omega)]^3$ refers to the test space for the velocity components (U, V) and temperature (θ), $Q=L_2(\Omega)$ refers to the test space for pressure component. Thus the weak formulation of Eqs. (3.9) to (3.12) are given as follow;

Find $(U,V,\theta)\in\mathbf{W}$ and $P\in Q$ such that,

$$\int_\Omega\left(U\frac{\partial U}{\partial X}+V\frac{\partial U}{\partial Y}\right)\widetilde{w}d\Omega+\int_\Omega\frac{\partial P}{\partial X}\widetilde{w}d\Omega-\Delta_1\int_\Omega\left(\frac{\partial^2U}{\partial X^2}+\frac{\partial^2U}{\partial Y^2}\right)\widetilde{w}d\Omega=0, \tag{3.13}$$

$$\begin{aligned}&\int_\Omega\left(U\frac{\partial V}{\partial X}+V\frac{\partial V}{\partial Y}\right)\widetilde{w}d\Omega+\int_\Omega\frac{\partial P}{\partial Y}\widetilde{w}d\Omega-\Delta_1\int_\Omega\left(\frac{\partial^2V}{\partial X^2}+\frac{\partial^2V}{\partial Y^2}\right)\widetilde{w}d\Omega\\&-\Delta_2\int_\Omega\theta\widetilde{w}d\Omega+\Delta_3\int_\Omega V\widetilde{w}d\Omega=0,\end{aligned} \tag{3.14}$$

$$\int_\Omega\left(\frac{\partial U}{\partial X}+\frac{\partial V}{\partial Y}\right)\widetilde{q}d\Omega=0, \tag{3.15}$$

$$\int_\Omega\left(U\frac{\partial \theta}{\partial X}+V\frac{\partial \theta}{\partial Y}\right)\widetilde{w}d\Omega-\Delta_4\int_\Omega\left(\frac{\partial^2\theta}{\partial X^2}+\frac{\partial^2\theta}{\partial Y^2}\right)\widetilde{w}d\Omega-\Delta_5\int_\Omega V^2\widetilde{w}d\Omega=0. \tag{3.16}$$

for all $(\widetilde{w}, \widetilde{q}) \in \mathbf{W} \times Q$

For the Galerkin discretization, infinite dimensional test and trial spaces are approximated by the finite dimensional test and trial spaces that is

$\mathbf{W} \approx \mathbf{W_h}$ and $Q \approx Q_h$

In the next step, we use Green's theorem to lower the order of derivatives for the trial function.

$$\Delta_1 \int_\Omega \left(\frac{\partial U_h}{\partial X}\frac{\partial \widetilde{w}_h}{\partial X} + \frac{\partial U_h}{\partial Y}\frac{\partial \widetilde{w}_h}{\partial Y} \right) d\Omega + \int_\Omega \left(U_h \frac{\partial U_h}{\partial X} + V_h \frac{\partial U_h}{\partial Y} \right) \widetilde{w}_h d\Omega - \int_\Omega \frac{\partial \widetilde{w}_h}{\partial X} P_h d\Omega = 0, \tag{3.17}$$

$$\Delta_1 \int_\Omega \left(\frac{\partial V_h}{\partial X}\frac{\partial \widetilde{w}_h}{\partial X} + \frac{\partial V_h}{\partial Y}\frac{\partial \widetilde{w}_h}{\partial Y} \right) d\Omega + \int_\Omega \left(U_h \frac{\partial V_h}{\partial X} + V_h \frac{\partial V_h}{\partial Y} \right) \widetilde{w}_h d\Omega + \Delta_3 \int_\Omega V_h \widetilde{w}_h d\Omega - \int_\Omega \frac{\partial \widetilde{w}_h}{\partial Y} P_h d\Omega - \Delta_2 \int_\Omega \theta_h \widetilde{w}_h d\Omega = 0, \tag{3.18}$$

$$\int_\Omega \frac{\partial U_h}{\partial X} \widetilde{q}_h d\Omega + \int_\Omega \frac{\partial V_h}{\partial Y} \widetilde{q}_h d\Omega = 0, \tag{3.19}$$

$$\Delta_4 \int_\Omega \left(\frac{\partial \theta_h}{\partial X}\frac{\partial \widetilde{w}_h}{\partial X} + \frac{\partial \theta_h}{\partial Y}\frac{\partial \widetilde{w}_h}{\partial Y} \right) d\Omega + \int_\Omega \left(U_h \frac{\partial \theta_h}{\partial X} + V_h \frac{\partial \theta_h}{\partial Y} \right) \widetilde{w}_h d\Omega - \Delta_5 \underline{\mathrm{V}} \int_\Omega V_h \widetilde{w}_h d\Omega = 0 \tag{3.20}$$

where

$$U_h = \sum_{j=1}^{n} U_j \zeta_j, \qquad V_h = \sum_{j=1}^{n} V_j \zeta_j, \qquad \theta_h = \sum_{j=1}^{n} \theta_j \zeta_j, \qquad P_h = \sum_{j=1}^{m} P_j \psi_j$$

represent the FEM approximate trial functions. Similarly,

$$\widetilde{w}_h = \sum_{i=1}^{n} \widetilde{w}_i \zeta_i \quad , \quad \widetilde{q}_h = \sum_{i=1}^{m} \widetilde{q}_i \psi_i$$

denote the approximated test functions.

Substituting these approximations for the trial and test functions in the Eqs. (3.17) to (3.20), the discretized system matrix can be written as

$$\underbrace{\begin{bmatrix} K^{11} & K^{12} & K^{13} & K^{14} \\ K^{21} & K^{22} & K^{23} & K^{24} \\ K^{31} & K^{32} & K^{33} & K^{34} \\ K^{41} & K^{42} & K^{43} & K^{44} \end{bmatrix}}_{A^*} \underbrace{\begin{bmatrix} \underline{U} \\ \underline{V} \\ \underline{P} \\ \underline{\theta} \end{bmatrix}}_{U^*} = \underbrace{\begin{bmatrix} \underline{F^1} \\ \underline{F^2} \\ \underline{F^3} \\ \underline{F^4} \end{bmatrix}}_{F^*} \tag{3.21}$$

where A^* is block matric, U^* is block vector and F^* denotes the associated block vector for the R.H.S. In block matrix,

$$K_{ij}^{11} = \Delta_1 \int_\Omega \left(\frac{\partial \zeta_j}{\partial X} \frac{\partial \zeta_i}{\partial X} + \frac{\partial \zeta_j}{\partial Y} \frac{\partial \zeta_i}{\partial Y} \right) d\Omega + \int_\Omega \left(\sum_{j=1}^{n} U_j \zeta_j \frac{\partial \zeta_j}{\partial X} + \sum_{j=1}^{n} V_j \zeta_j \frac{\partial \zeta_j}{\partial Y} \right) \zeta_i d\Omega,$$

$$K_{ij}^{22} = \Delta_1 \int_\Omega \left(\frac{\partial \zeta_j}{\partial X} \frac{\partial \zeta_i}{\partial X} + \frac{\partial \zeta_j}{\partial Y} \frac{\partial \zeta_i}{\partial Y} \right) d\Omega + \int_\Omega \left(\sum_{j=1}^{n} U_j \zeta_j \frac{\partial \zeta_j}{\partial X} + \sum_{j=1}^{n} V_j \zeta_j \frac{\partial \zeta_j}{\partial Y} \right) \zeta_i d\Omega,$$

$$K_{ij}^{44} = \Delta_4 \int_\Omega \left(\frac{\partial \zeta_j}{\partial X} \frac{\partial \zeta_i}{\partial X} + \frac{\partial \zeta_j}{\partial Y} \frac{\partial \zeta_i}{\partial Y} \right) d\Omega + \int_\Omega \left(\sum_{j=1}^{n} U_j \zeta_j \frac{\partial \zeta_j}{\partial X} + \sum_{j=1}^{n} V_j \zeta_j \frac{\partial \zeta_j}{\partial Y} \right) \zeta_i d\Omega,$$

$$K_{ij}^{13} = \int_\Omega \left(\frac{\partial \psi_j}{\partial X} \right) \zeta_i d\Omega, \quad K_{ij}^{23} = \int_\Omega \left(\frac{\partial \psi_j}{\partial y} \right) \zeta_i d\Omega, \quad K_{ij}^{31} = \int_\Omega \left(\frac{\partial \zeta_i}{\partial X} \right) \psi_j d\Omega$$

$$K_{ij}^{32} = \int_\Omega \left(\frac{\partial \zeta_i}{\partial X} \right) \psi_j d\Omega, \quad K_{ij}^{24} = \Delta_3 \int_\Omega \zeta_j \zeta_i d\Omega, \quad K_{ij}^{42} = -\Delta_5 \, \underline{\mathrm{V}} \int_\Omega \zeta_j \zeta_i d\Omega,$$

$$K_{ij}^{12} = K_{ij}^{14} = K_{ij}^{21} = K_{ij}^{33} = K_{ij}^{34} = K_{ij}^{41} = K_{ij}^{43} = 0$$

Velocity and temperature components are discretized by Q_2 element having $3rd$ order accuracy and P_1^{disc} element of $2nd$ order accuracy in L_2-norm respectively is used for the discretization of pressure component. The discretized non-linear partial differential equations linearized by using picard iteration method and then

Gaussian elimination method has been used to solved the related linearized systems. The convergence of solution is assumed when the relative residual for each dependent variable fulfils the following stoping criteria.

$$\left| \frac{\Upsilon^{n+1} - \Upsilon^{n}}{\Upsilon^{n+1}} \right| \leq 10^{-6}$$

where Υ denotes the dependent variable U, V, P, θ and n represents the number of iteration.

Grid Generation and Refinement

First of all, the coarsest mesh with four cells at level $\ell = 1$, which is further refined into small cells by joining the midpoints of opposite faces of current cell denoted by the following $\ell = \ell + 1$ can be achieved by dividing each cell into further four new cells elaborated in Figure 3.2

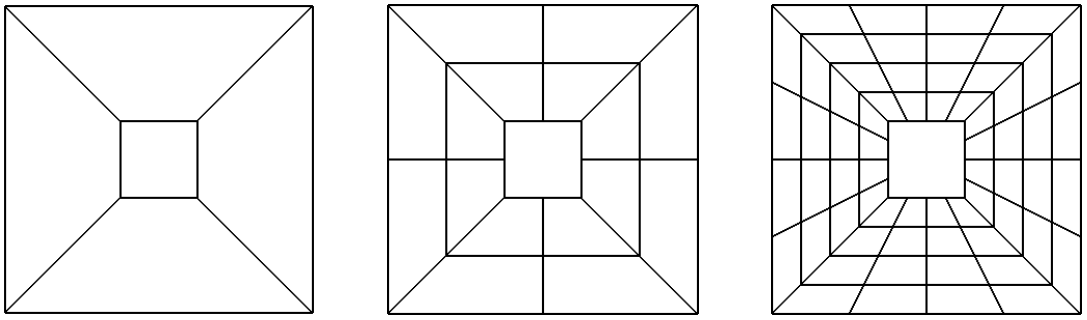

Figure 3.2: Pattern of grids on space mesh level = 1,2,3 (from left to right)

3.3 Code Validation

Table 3.2 represents the code validation for the mixed convection flow where it can be seen that result have very good agreement with published results in the literature. In the addition, Table 3.3 demonstrates comparison of the Nu_{avg} obtained the present study and the numerical results found in the literature [20] for a particular case of mixed convection in an enclosure having isothermal cylinder.

Re	Present Study	Ref. [26]	Ref. [39]	Ref. [36]	Ref. [45]	Ref. [1]	Ref. [37]	Ref. [22]
100	2.03	–	2.05	2.01	–	2.09	–	1.94
400	4.07	4.08	4.09	3.97	4.14	4.16	4.05	3.84
1000	6.58	6.48	6.70	6.28	6.61	6.55	6.55	6.33

Table 3.2: Comparison of present result with some above mentioned results

Nu_{avg}	Ri	Present Study	Ref. [20]
	0.1	5.2223	5.6118
	1.0	5.2339	5.6935
	10	6.06844	7.9083

Table 3.3: Comparison of present result with the result of isothermal hot obstacle in a cavity

Grid Independence Test

Table 3.4 shows the grid convergence test at different mesh level (ℓ) to compute the Nusselt number for $Ha = 25,\ Pr = 6.2,\ \phi = 0.2,\ Ec = 10^{-4}$ and $Re = 100$ along with total number of all spaces degree of freedom (#DOFs) and number of element (#EL) which are required for the definition of discreet velocity, pressure and temperature with respect to used discretization.

ℓ	#EL	#DOFs	$Nu_{avg}(Ri = 1)$	$Nu_{avg}(Ri = 10)$
3	64	1056	4.4599711	7.081795
4	256	4032	5.1383737	8.3907139
5	1024	15744	5.5082335	9.1507667
6	4096	62208	5.6700676	9.5341186
7	16384	247296	5.7415596	9.7194242

Table 3.4: Grid independence results for the proposed configuration.

3.4 Results and Discussions

Here we examine the impact of magnetic field on the mixed convection in alumina-water nanofluid poured with in the square enclosure having isothermal blockage with standard values ($Ec = 10^{-4}$, $Ha = 25$, $\phi = 0.2$, $Pr = 6.2$ and $Re = 100$). These values have been taken in account unless different parameters values are given and for the present study $Ri = 1$ (mixed convection), $Ri = 0.1$ (forced convection) and $Ri = 10$ (natural convection) are used.

Figure 3.3 displays an impact of the different Ha on the isotherms and streamlines for $Ri = 0.1$. At $Ha = 0$, in the absences of magnetic field clockwise recirculating eddy above the obstacle near the upper edge of the enclosure has been sighted. Most of the streamlines are highly distributed near the upper movable surface indicating that velocity of fluid is high in this region while coarser distribution of the streamline have been observed far away from the upper movable surface. As magnetic field approaches to $Ha = 25$, the circulation of flow decreases which is indicated reduction in the flow of fluid and mostly streamlines appears close to the upper movable wall and above the central square cylinder. For $Ha = 50$ and 100, all streamlines are limited to the small portion like plume manner above the square cylinder showing a drop-off in the fluid flows into the cavity, due to the presence of magnetic field as Lorentz force is produced in the opposite direction of flow.

At $Ha = 0$, when magnetic field does not play its role at that value isotherms are assembled close to the lower edge and nearby square cylinder indicating that temperature gradient is higher in this zone. Isotherms are shifted towards the left side of upper adiabatic surface because of shear forces. Therefore, thermal boundary layer occurs in this zone. A mild change has been noticed in the behavior of isotherms and most of the isotherms becomes parallel to the heated lower surface for $Ha = 0$.

Figure 3.4 demonstrates the influence of mixed convection mode for different values of Ha on the isotherms and streamlines. Shear flow is produced because the upper moving surface while buoyancy-force is generated due to hot lower surface

or isothermal square cylinder. Here both forces have equal impact on the temperature distribution and flow field. When magnetic field has no effect at $Ha = 0$, more streamlines are crowded together around the central blockage showing that buoyancy-force is dominated in this zone. Moreover increasing the $Ha = 25$ from $Ha = 0$, numbers of coarsely spreaded streamlines across the blockage is observed comparatively less but that has been noticed more in case of forced convection mode, which indicates the decrease of fluid velocity in the cavity. By increasing the strength of magnetic field at $Ha = 50$ and 100, streamlines gatherings to the upper surface and is limited to a small zone that shows velocity of flow is reduced. The behavior of isotherm changes slightly in comparison to the case of $Ri = 0.1$ (forced convection).

Figure 3.5 illuminates the effect on isotherms and streamlines for the variations of Hartmann number. At $Ri = 10$ natural or free convection occurs, here buoyancy-force is leading over shear-force. In the absence of magnetic field, the streamlines are almost equally spread and are slightly stretched obliquely to the upper right edge because of the motion of upper surface, whereas movement of fluid occurs due to the hot lower surface. circulation of rotating eddy becomes weak in the center of the enclosure across the blockage which indicates a decline in the flow of liquid in that zone. By increasing the magnetic field to $Ha = 25$, clockwise rotation of eddy has been moved up to the square block that indicates the reduction in flow. For $Ha = 50$, circulation of streamlines are coarsely across right, left and the lower surface of the square cylinder has been noticed. At $Ha = 100$, most of the streamlines are elongates near the upper wall above obstacle which shows that the flow of fluid is decline in this area. The isotherms are strictly spaced close the hot lower surface and across heated square block. Which indicates enlargement of thin boundary layer and extreme temperature gradient over the lower surface and the square cylinder.

Figure 3.6 exhibits the impact of Richardson's number on isotherms and streamlines for $Ec = 10^{-2}$. For the forced convection at $Ri = 0.01$, shear-driven flow is leading in the enclosure and the most of the streamlines are restraint the upper movable surface. Enhancement of Ri up to 1, buoyancy and shear forces play

equal role so more streamlines notice near the lower surface. As raised up Ri from 1 to 10, the motion of fluids has been noticed in the enclosure across the square cylinder because of the natural convection. Isotherms shift through non-adjacent vertices of adiabatic walls and gathered across the uniformly heated square block for $Ri = 0.1$. For mixed convection, the isotherms are crowded together near the lower hot surface. In natural convection mode ($Ri = 10$), mostly isotherms become parallel to the lower surface because of the influential forces of buoyancy.

Figure 3.7(a-b) exhibits the influence of Ec for different modes of convection on Nu_{avg} and θ_{avg}. As we considered limited fluctuation of Eckert number ($Ec = 10^{-4}, 10^{-3}, 10^{-2}$), hence mild effect has been noticed in all the three cases of convection. There is no change observed in Nu_{avg} by increasing Eckert number in Figure 3.7(a). Ec develop an intensification in average temperature in square enclosure that can be viewed in Figure. 3.7(b).

Figure 3.8(a) and (b) illustrates the Nu_{avg} and θ_{avg} as a function of different H for $Re = 1, 10, 100$. Figure. 3.8(a) shows that Nu_{avg} reduces by enhancing the magnetic field strength. It is due to the dominant of shear force under the influence of magnetic field as compared to the buoyancy induced flow in the cavity. Figure. 3.8(b) delineates that increasing the Hartmann number average temperature is slightly increased for $Re = 0.1, 10$ but for $Re = 100$ first reduction appears and after some value it shows the large augmentation in θ_{avg}.

Figure 3.9(a-b) demonstrate the impact of various Ha on the Nu_{avg} and θ_{avg} for three regimes of convection at $Ri = 0.1, 1$ and 10. As enhancing the magnitude of magnetic field for all three modes of convection ($Ri = 0.1, 1, 10$) causes to decline the Nu_{avg} which can be visualized from Figure 3.9(a). There is an improvement of average temperature distribution in the enclosure with increasing the Hartmann number which can be visualized from Figure. 3.9(b).

Figure 3.10(a) illuminate the impact of Ec on Nu_{avg} as a function ϕ, which indicates that Nu_{avg} increases with enhancement of volume fraction of nanoparticles. Effect of ϕ on average temperature distribution as a function of Ec is depicted in Figure 3.10(b). It is noticed that by the growth of Ec, θ_{avg} is increasing.

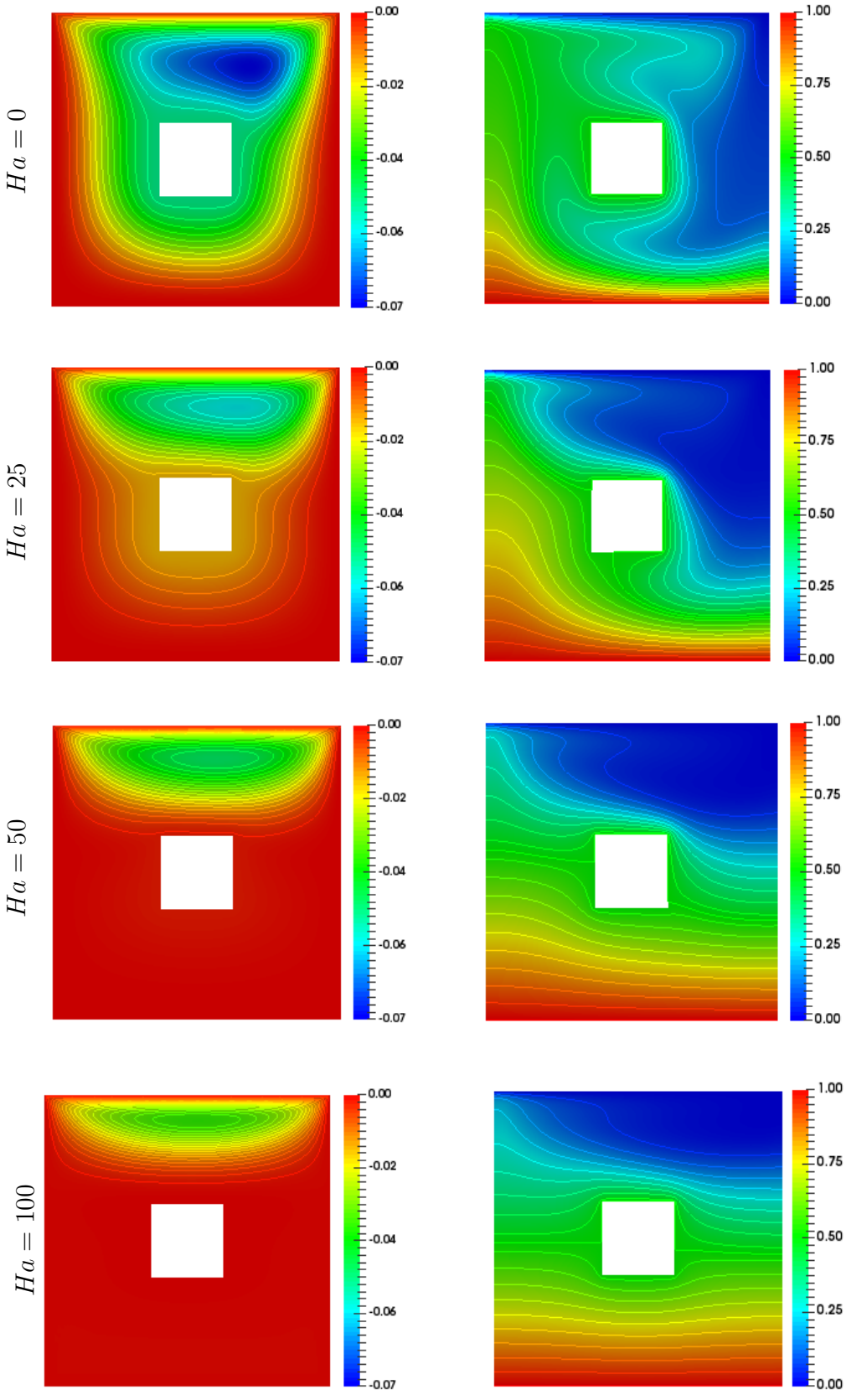

Figure 3.3: Streamlines (a) and isotherms (b) for different Ha at $Ri = 0.1$.

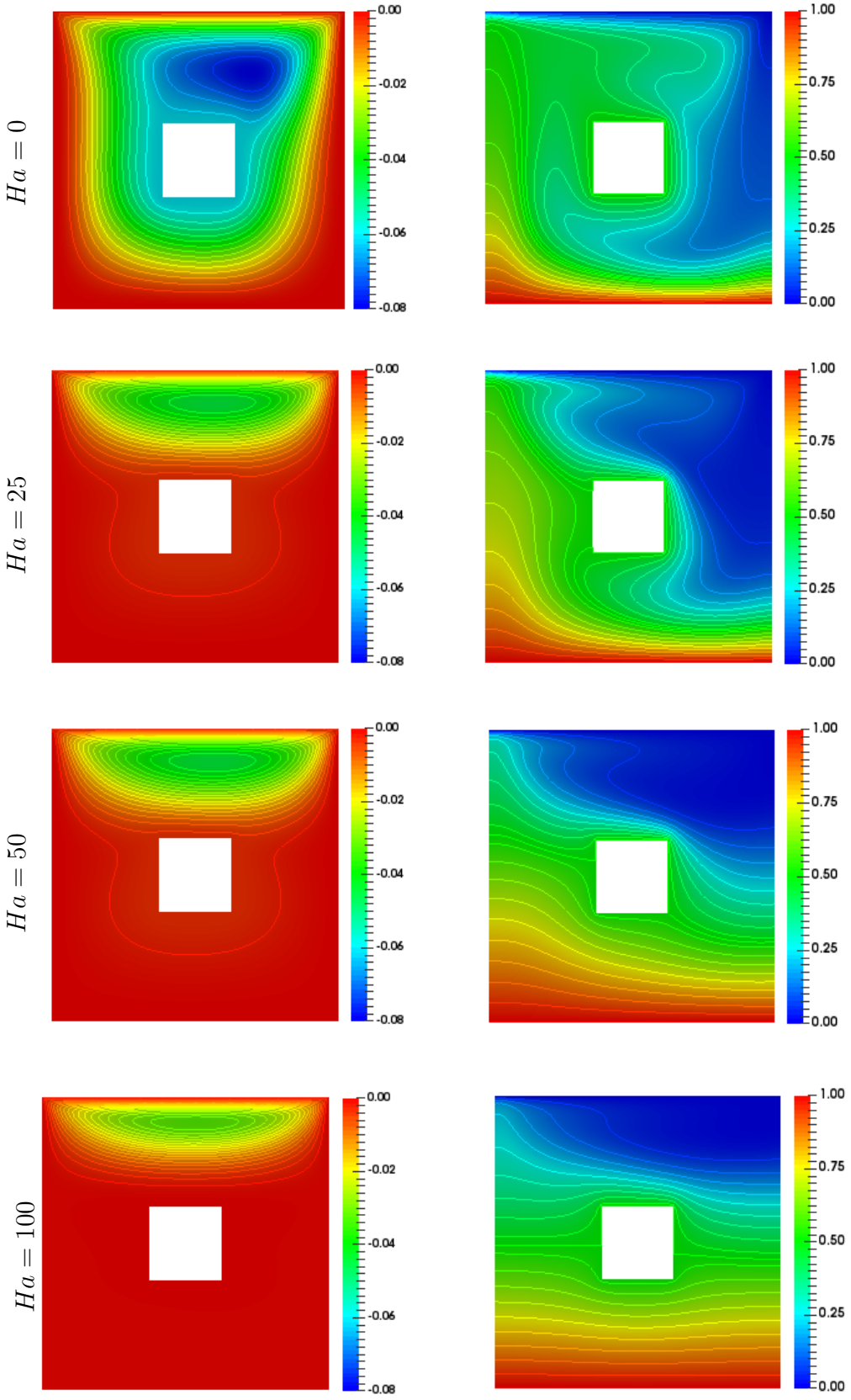

Figure 3.4: Streamlines (a) and isotherms (b) for different Ha at $Ri = 1$.

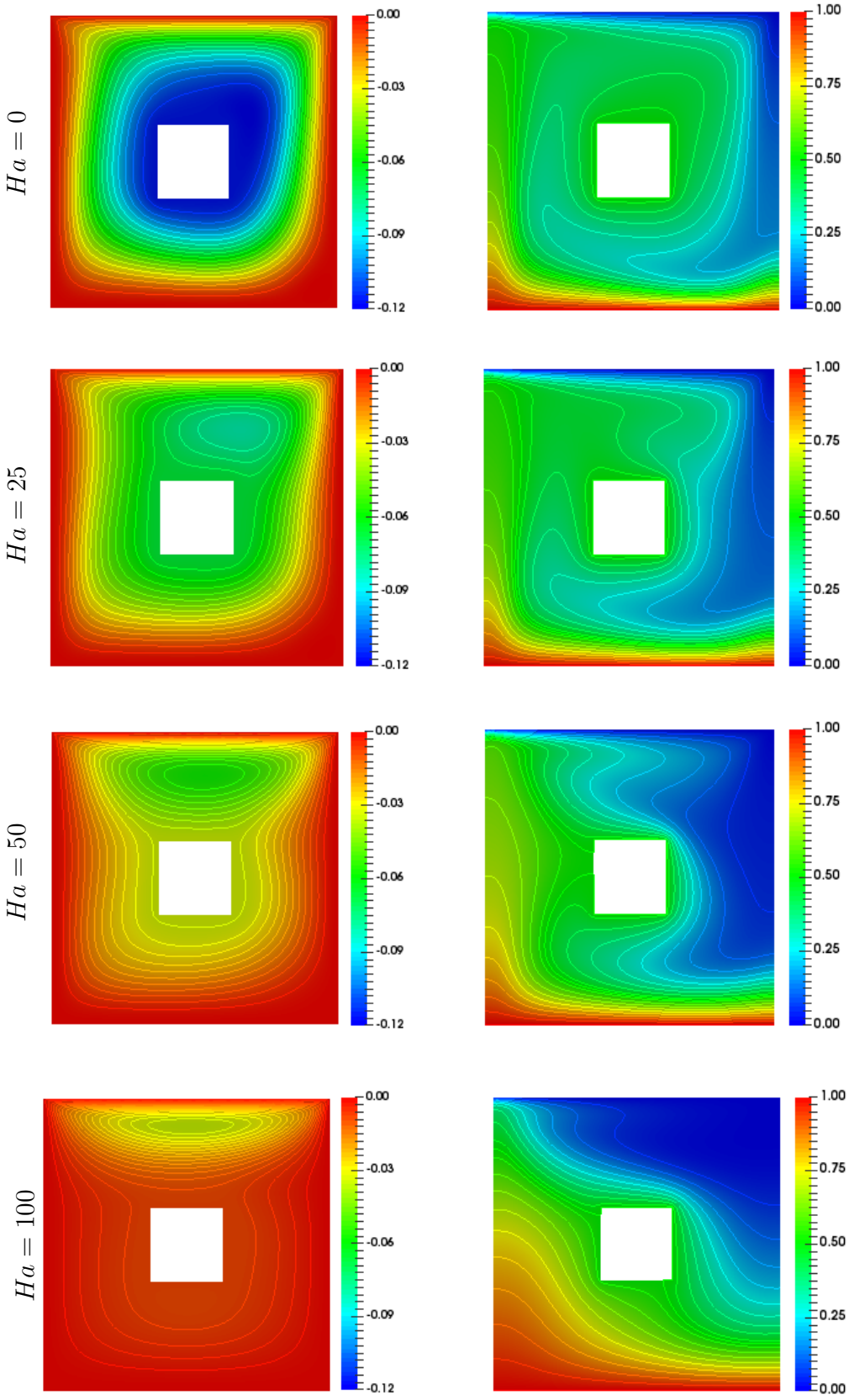

Figure 3.5: Streamlines (a) and isotherms (b) for different Ha at $Ri = 10$.

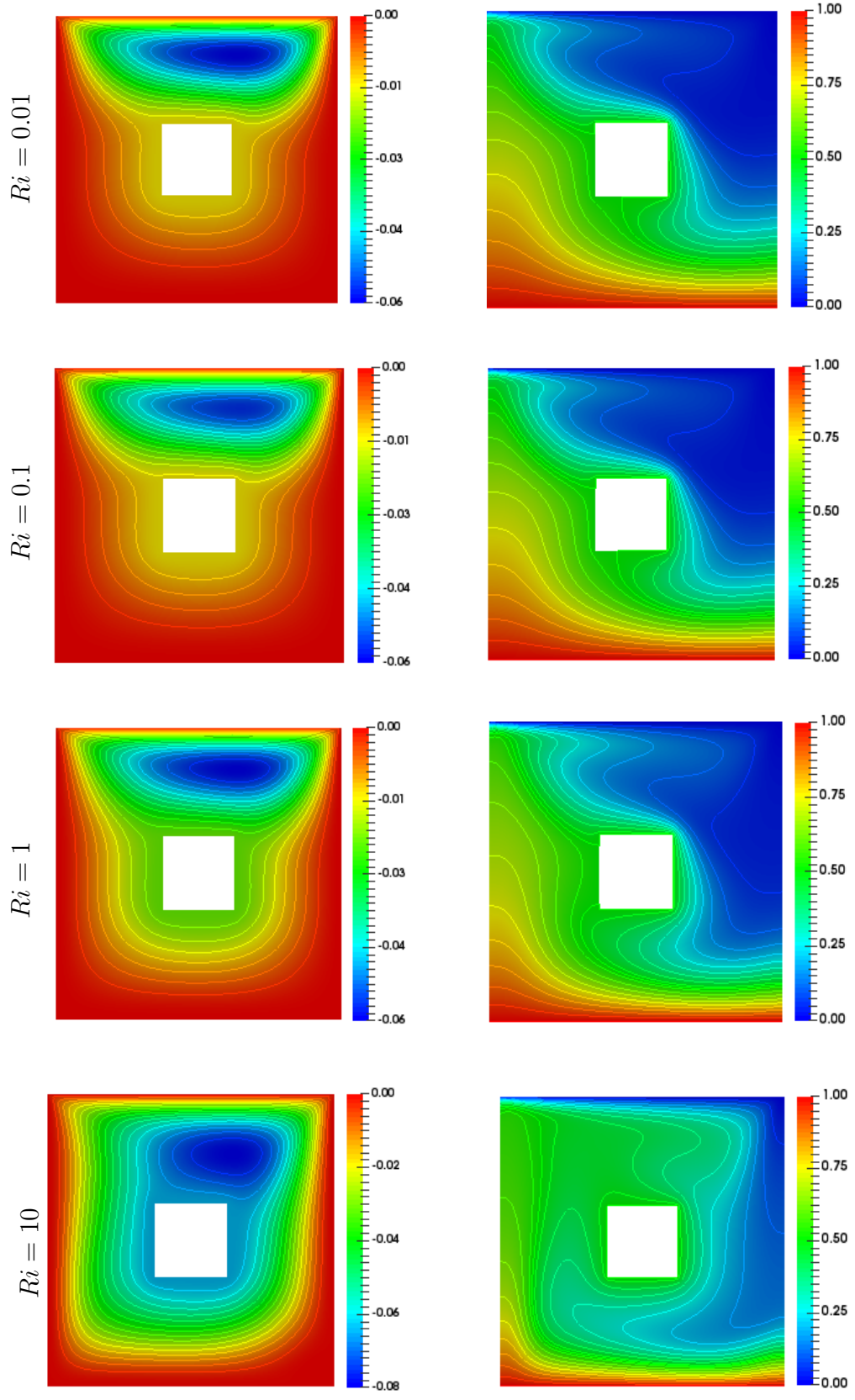

(a) (b)

Figure 3.6: Streamlines (a) and isotherms (b) for different modes of convection at $Ec = 10^{-2}$.

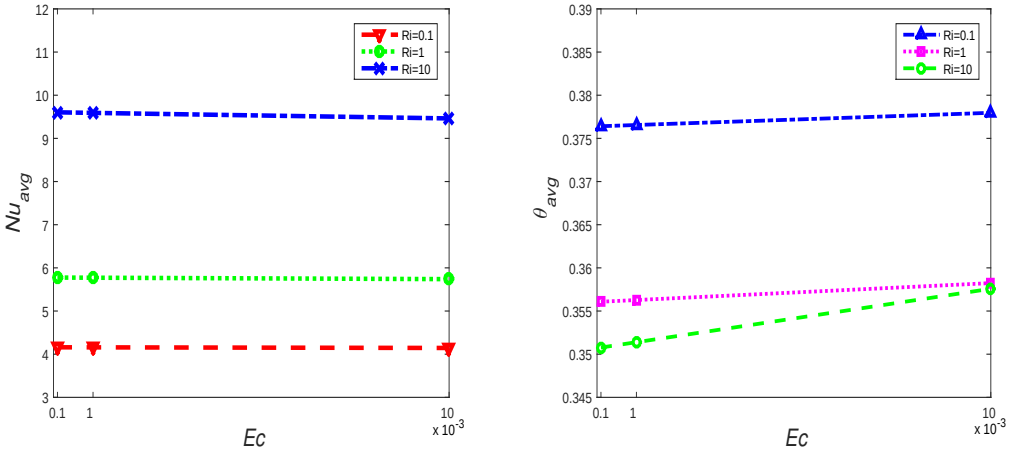

(a) (b)

Figure 3.7: Variation of Nu_{avg} and θ_{avg} as a function of Ec for different Ri.

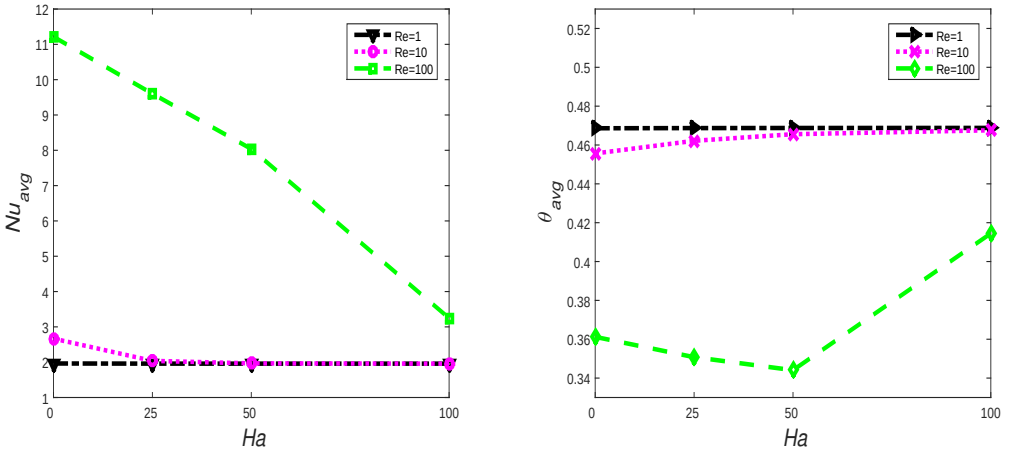

(a) (b)

Figure 3.8: Variation of Nu_{avg} and θ_{avg} as a function of Ha for different Re.

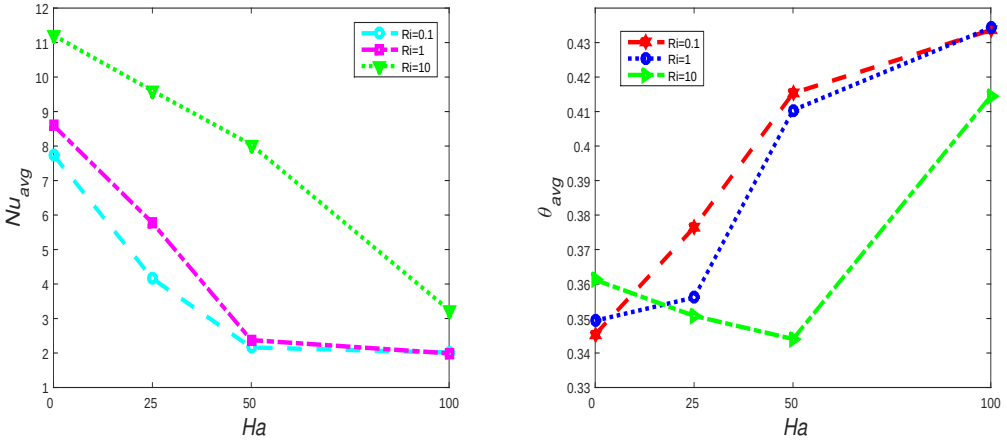

(a) (b)

Figure 3.9: Variation of Nu_{avg} and θ_{avg} as a function of Ha for different Ri.

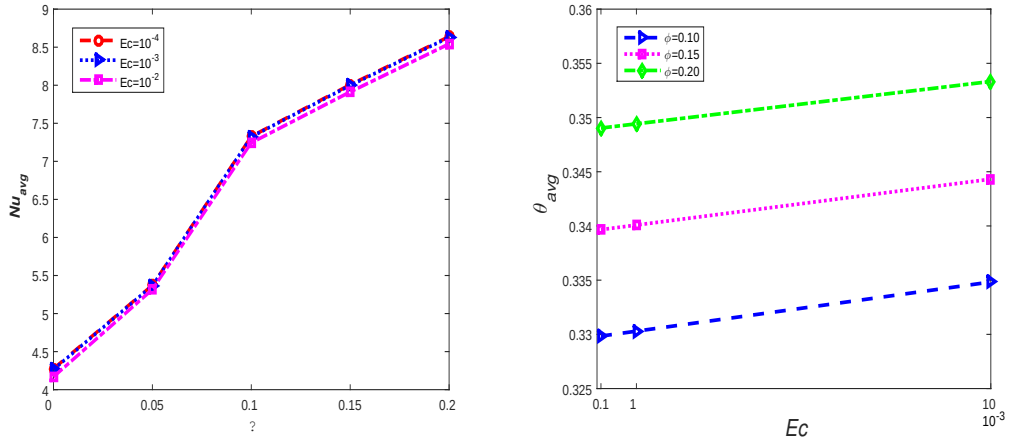

(a) (b)

Figure 3.10: Variation of Nu_{avg} and θ_{avg} as a function of Ec and ϕ.

Chapter 4

Simulation of MHD Mixed Convection Nanofluid Flow in a Cavity with an Obstacle and Non-Linear Thermal Radiations

Based on the literature review, many researchers have analyzed MHD mixed convection in a cavity having obstacles of different shape. Previously, impact of different physical parameters on the rate of heat transport have been observed but in spite of all considered work, there is very rare information regarding MHD on combined convection in an enclosure having obstacle coupled with non-linear thermal radiations. The main purpose of this chapter is to extend the work of Mehmood *et al.* [27] and perform the numerical simulation to analyze the effect of non-linear thermal radiations on heat transfer phenomena and fluid flow through isotherms and streamlines.

4.1 Problem Description

The system to be explored is a two-dimensional, steady and laminar flow of Newtonian and incompressible fluid in a driven enclosure with an isothermal square obstacle together with non-linear thermal radiations. The viscous dissipation and induced electric current are neglected in the present study [38] while Joule heating coupled with non-linear thermal radiations are taken into account in the energy equation. Physical model along with boundary conditions of proposed work is portrayed in Figure 3.1. The upper surface of the enclosure is moving with uniform velocity U_L along the positive $x-$axis. Temperature of lower and upper surfaces of the cavity are maintained as T_h and T_c where $T_h > T_c$ while the side walls are kept adiabatic and uniform average temperature $(\frac{T_h+T_c}{2})$ is maintained for the central obstacle. Thermo-physical properties of Aluminium particles are kept constant (see Table 3.1). The basic fundamental laws utilized to solve the proposed flow problem are the laws of conservation of mass, momentum, energy, which establish a set of coupled non-linear PDEs. In the present work non-linear thermal radiations have been taken into account in the energy equation. Boussinesq approximation has been adopted for the buoyancy term in momentum equation and radiative thermal heat flux is modeled on the basis of Rosseland approximation [35]

$$q_{rx} = \frac{-4\sigma^*}{k^*}\frac{\partial T^4}{\partial x} = \frac{-16\sigma_*}{3a_R}T^3\frac{\partial T}{\partial x}$$

$$q_{ry} = \frac{-4\sigma^*}{k^*}\frac{\partial T^4}{\partial y} = \frac{-16\sigma_*}{3a_R}T^3\frac{\partial T}{\partial y}$$

4.1.1 Dimensional Governing Equations

Under on the aforementioned assumptions for the proposed problem the dimensional governing PDEs can be write as:

- Continuity Equation:

$$\frac{\partial u}{\partial x} + \frac{\partial v}{\partial y} = 0 \tag{4.1}$$

- x Momentum Equation:

$$u\frac{\partial u}{\partial x} + v\frac{\partial u}{\partial y} = -\frac{1}{\rho_{nf}}\frac{\partial p}{\partial x} + \frac{\mu_{nf}}{\rho_{nf}}\left(\frac{\partial^2 u}{\partial x^2} + \frac{\partial^2 u}{\partial y^2}\right) \tag{4.2}$$

- y Momentum Equation:

$$u\frac{\partial v}{\partial x} + v\frac{\partial v}{\partial y} = -\frac{1}{\rho_{nf}}\frac{\partial p}{\partial y} + \frac{\mu_{nf}}{\rho_{nf}}\left(\frac{\partial^2 v}{\partial x^2} + \frac{\partial^2 v}{\partial y^2}\right) + \frac{(\rho\beta)_{nf}}{\rho_{nf}} g\,(T - T_c) - \frac{\sigma_{nf} B_0^2}{\rho_{nf}} v \tag{4.3}$$

- Energy Equation:

$$u\frac{\partial T}{\partial x} + v\frac{\partial T}{\partial y} = \alpha_{nf}\left(\frac{\partial^2 T}{\partial x^2} + \frac{\partial^2 T}{\partial y^2}\right) + \frac{\sigma_{nf} B_0^2}{(\rho C_p)_{nf}} v^2 - \frac{1}{(\rho C_p)_{nf}}\left(\frac{\partial q_{rx}}{\partial x} + \frac{\partial q_{ry}}{\partial y}\right) \tag{4.4}$$

4.1.2 Dimensional Boundary Conditions

Dimensional boundary conditions on each wall of the cavity and isothermal blockage for temperature field and velocity can be written as:

- On the top wall of square enclosure:

$$u(x, y) = U_L, \quad v(x, y) = 0, \quad T = T_c$$

- On the bottom wall of square cavity:

$$u(x, y) = 0, \quad v(x, y) = 0, \quad T = T_h$$

- On the vertical walls of square enclosure:

$$u(x, y) = 0, \quad v(x, y) = 0, \quad \frac{\partial T}{\partial x} = 0$$

- On the blockage inside the cavity:

$$u(x,y)=0, \quad v(x,y)=0, \quad T=\frac{T_h+T_c}{2}$$

4.1.3 Non-Dimensional Analysis

The following non-dimensional parameter are used to reduces the governing Eqs (4.1) to (4.4) into non-dimensional form as follows,

$$X=\frac{x}{\widetilde{L}}, \quad Y=\frac{y}{\widetilde{L}}, \quad U=\frac{u}{U_L}, \quad V=\frac{v}{U_L}, \quad \theta=\frac{T-T_c}{T_h-T_c}, \quad P=\frac{p}{\rho_{nf}{U_L}^2}$$
$$Re=\frac{U_L\widetilde{L}}{\nu_f}, \quad Gr=\frac{g\beta_f(T_h-T_c)\widetilde{L}^3}{\nu_f^2}, \quad Ha=B_0\widetilde{L}\sqrt{\frac{\sigma_f}{\mu_f}}, \quad Pr=\frac{\nu_f}{\alpha_f}$$
$$Ri=\frac{Gr}{Re^2}, \quad Ec=\frac{{U_L}^2}{(C_p)_f(T_h-T_c)}, \quad Rd=\frac{4\sigma^*{T_c}^3}{k^*k_f}, \quad Nr=\frac{T_h}{T_c}.$$

The transformed non-dimensional governing equations can be expressed as follows,

$$\frac{\partial U}{\partial X}+\frac{\partial V}{\partial Y}=0, \tag{4.5}$$

$$U\frac{\partial U}{\partial X}+V\frac{\partial U}{\partial Y}=-\frac{\partial P}{\partial X}+\frac{1}{Re}\frac{\rho_f}{\rho_{nf}}\frac{1}{(1-\phi)^{2.5}}\left(\frac{\partial^2 U}{\partial X^2}+\frac{\partial^2 U}{\partial Y^2}\right), \tag{4.6}$$

$$\begin{aligned}U\frac{\partial V}{\partial X}+V\frac{\partial V}{\partial Y}=&-\frac{\partial P}{\partial Y}+\frac{1}{Re}\frac{\rho_f}{\rho_{nf}}\frac{1}{(1-\phi)^{2.5}}\left(\frac{\partial^2 V}{\partial X^2}+\frac{\partial^2 V}{\partial Y^2}\right)\\&+Ri\frac{\rho_f}{\rho_{nf}}\big(1-\phi+\frac{\rho_s\beta s}{\rho_f\beta_f}\phi\big)\theta-\frac{\rho_f}{\rho_{nf}}\frac{\sigma_{nf}}{\sigma_f}\frac{Ha^2}{Re}V,\end{aligned} \tag{4.7}$$

$$\begin{aligned}U\frac{\partial \theta}{\partial X}+V\frac{\partial \theta}{\partial Y}=&\frac{1}{RePr}\left\{\frac{\alpha_{nf}}{\alpha_f}+\frac{(\rho C_p)_f}{(\rho C_p)_{nf}}\frac{4}{3}Rd\left(\theta(Nr-1)+1\right)^3\right\}\left(\frac{\partial^2\theta}{\partial X^2}+\frac{\partial^2\theta}{\partial Y^2}\right)\\&+\frac{Ha^2Ec}{Re}\frac{\sigma_{nf}}{\sigma_f}\frac{(\rho C_p)_f}{(\rho C_p)_{nf}}V^2.\end{aligned} \tag{4.8}$$

4.1.4 Boundary Conditions (Dimensionless)

The associated boundary conditions for dimensionless velocity and temperature field along each side of square enclosure and heated obstacle are reduced as follows,

- On the top wall of cavity:

$$U(X,Y) = 1, \quad V(X,Y) = 0, \quad \theta = 0$$

- On the bottom wall of cavity:

$$U(X,Y) = 0, \quad V(X,Y) = 0, \quad \theta = 1$$

- On the left and right wall of cavity:

$$U(X,Y) = 0, \quad V(X,Y) = 0, \quad \frac{\partial \theta}{\partial X} = 0$$

- On the blockage inside the cavity:

$$U(X,Y) = 0, \quad V(X,Y) = 0, \quad \theta = \frac{1}{2}$$

Physical Quantities of Interest

Nusselt number is important for the analysis of flow of fluid and heat transfer, it also tells the quality of heat transport phenomena rather than its quantity. Local and average Nusselt number including the non-linear thermal radiation can be obtained as follow,
Local Nusselt number is given by

$$Nu = -\left(\frac{k_{nf}}{k_f} + \frac{4}{3}RdNr^3\right)\left(\frac{\partial \theta}{\partial Y}\right)|_{Y=0}.$$

Average Nusselt number is given by

$$Nu_{avg} = \int_0^1 Nu dx.$$

4.2 Numerical Solution

GFEM has been adopted to discretized the set of coupled non-linear dimensionless Eqs (4.5) to (4.8) subjected to associated boundary conditions.

4.2.1 Variational/Weak Formulation

The basic feature of FEM is to transform the strong form of non-linear PDE's into weak formulation. As strong form is not always give refine solution of concerned problem and also makes stability issue so to overcome this difficulty variational form is adopted. The main idea of variational form is to transform the set of coupled non-dimensional equations by multiply with suitable test function and then performed integration whole over the domain (Ω). Strong form can be re-write as,

$$U\frac{\partial U}{\partial X}+V\frac{\partial U}{\partial Y}=-\frac{\partial P}{\partial X}+\Delta_1\left(\frac{\partial^2 U}{\partial X^2}+\frac{\partial^2 U}{\partial Y^2}\right), \tag{4.9}$$

$$U\frac{\partial V}{\partial X}+V\frac{\partial V}{\partial Y}=-\frac{\partial P}{\partial Y}+\Delta_1\left(\frac{\partial^2 V}{\partial X^2}+\frac{\partial^2 V}{\partial Y^2}\right)+\Delta_2\theta-\Delta_3 V, \tag{4.10}$$

$$\frac{\partial U}{\partial X}+\frac{\partial V}{\partial Y}=0, \tag{4.11}$$

$$U\frac{\partial \theta}{\partial X}+V\frac{\partial \theta}{\partial Y}=\Delta_4\left(\frac{\partial^2 \theta}{\partial X^2}+\frac{\partial^2 \theta}{\partial Y^2}\right)+\Delta_5 V^2. \tag{4.12}$$

where Δ_i's in the above equations are given by;

$$\Delta_1=\frac{1}{Re}\frac{\rho_f}{\rho_{nf}}\frac{1}{(1-\phi)^{2.5}},\quad \Delta_2=Ri\frac{\rho_f}{\rho_{nf}}\left(1-\phi+\frac{\rho_s\beta s}{\rho_f\beta_f}\phi\right),\quad \Delta_3=\frac{\rho_f}{\rho_{nf}}\frac{\sigma_{nf}}{\sigma_f}\frac{Ha^2}{Re},$$

$$\Delta_4=\frac{1}{RePr}\left\{\frac{\alpha_{nf}}{\alpha_f}+\frac{(\rho C_p)_f}{(\rho C_p)_{nf}}\frac{4}{3}Rd\left(\theta(Nr-1)+1\right)^3\right\},\quad \Delta_5=\frac{Ha^2Ec}{Re}\frac{\sigma_{nf}}{\sigma_f}\frac{(\rho C_p)_f}{(\rho C_p)_{nf}}.$$

In order to obtain the variational/weak formulation, first multiply both sides of the momentum, energy, and continuity equation with test functions $\widetilde{w} \in \mathbf{W}$ and $\widetilde{q} \in Q$ respectively, after this integration is performed whole over the entire domain (Ω). Thus the variational form of governing Eqs (4.11) to (4.12) can be read as follow;

Find $(U, V, \theta) \in \mathbf{W}$ and $P \in Q$ such that,

$$\int_{\Omega} \left(U\frac{\partial U}{\partial X} + V\frac{\partial U}{\partial Y} \right) \widetilde{w} d\Omega + \int_{\Omega} \frac{\partial P}{\partial X} \widetilde{w} d\Omega - \Delta_1 \int_{\Omega} \left(\frac{\partial^2 U}{\partial X^2} + \frac{\partial^2 U}{\partial Y^2} \right) \widetilde{w} d\Omega = 0, \tag{4.13}$$

$$\int_{\Omega} \left(U\frac{\partial V}{\partial X} + V\frac{\partial V}{\partial Y} \right) \widetilde{w} d\Omega + \int_{\Omega} \frac{\partial P}{\partial Y} \widetilde{w} d\Omega - \Delta_1 \int_{\Omega} \left(\frac{\partial^2 V}{\partial X^2} + \frac{\partial^2 V}{\partial Y^2} \right) \widetilde{w} d\Omega$$
$$- \Delta_2 \int_{\Omega} \theta \widetilde{w} d\Omega + \Delta_3 \int_{\Omega} V \widetilde{w} d\Omega = 0, \tag{4.14}$$

$$\int_{\Omega} \left(\frac{\partial U}{\partial X} + \frac{\partial V}{\partial Y} \right) \widetilde{q} d\Omega = 0, \tag{4.15}$$

$$\int_{\Omega} \left(U\frac{\partial \theta}{\partial X} + V\frac{\partial \theta}{\partial Y} \right) \widetilde{w} d\Omega - \Delta_4 \int_{\Omega} \left(\frac{\partial^2 \theta}{\partial X^2} + \frac{\partial^2 \theta}{\partial Y^2} \right) \widetilde{w} d\Omega - \Delta_5 \int_{\Omega} V^2 \widetilde{w} d\Omega = 0 \tag{4.16}$$

for all $(\widetilde{w}, \widetilde{q}) \in \mathbf{W} \times Q$

In Galerkin approximation infinite dimensional spaces are discretized into finite dimensional spaces,

$\mathbf{W} \approx \mathbf{W_h}$ and $Q \approx Q_h$

In the next step, we use Green's theorem to lower the order of derivatives for the trial function.

$$\Delta_1 \int_\Omega \left(\frac{\partial U_h}{\partial X}\frac{\partial \widetilde{w}_h}{\partial X} + \frac{\partial U_h}{\partial Y}\frac{\partial \widetilde{w}_h}{\partial Y} \right) d\Omega + \int_\Omega \left(U_h \frac{\partial U_h}{\partial X} + V_h \frac{\partial U_h}{\partial Y} \right) \widetilde{w}_h d\Omega - \int_\Omega \frac{\partial \widetilde{w}_h}{\partial X} P_h d\Omega = 0, \tag{4.17}$$

$$\Delta_1 \int_\Omega \left(\frac{\partial V_h}{\partial X}\frac{\partial \widetilde{w}_h}{\partial X} + \frac{\partial V_h}{\partial Y}\frac{\partial \widetilde{w}_h}{\partial Y} \right) d\Omega + \int_\Omega \left(U_h \frac{\partial V_h}{\partial X} + V_h \frac{\partial V_h}{\partial Y} \right) \widetilde{w}_h d\Omega + \Delta_3 \int_\Omega V_h \widetilde{w}_h d\Omega - \int_\Omega \frac{\partial \widetilde{w}_h}{\partial Y} P_h d\Omega - \Delta_2 \int_\Omega \theta_h \widetilde{w}_h d\Omega = 0, \tag{4.18}$$

$$\int_\Omega \frac{\partial U_h}{\partial X} \widetilde{q}_h d\Omega + \int_\Omega \frac{\partial V_h}{\partial Y} \widetilde{q}_h d\Omega = 0, \tag{4.19}$$

$$\Delta_4 \int_\Omega \left(\frac{\partial \theta_h}{\partial X}\frac{\partial \widetilde{w}_h}{\partial X} + \frac{\partial \theta_h}{\partial Y}\frac{\partial \widetilde{w}_h}{\partial Y} \right) d\Omega + \int_\Omega \left(U_h \frac{\partial \theta_h}{\partial X} + V_h \frac{\partial \theta_h}{\partial Y} \right) \widetilde{w}_h d\Omega - \Delta_5 \overline{\nabla} \int_\Omega V_h \widetilde{w}_h d\Omega = 0. \tag{4.20}$$

where

$$U_h = \sum_{j=1}^{n} U_j \zeta_j, \qquad V_h = \sum_{j=1}^{n} V_j \zeta_j, \qquad \theta_h = \sum_{j=1}^{n} \theta_j \zeta_j, \qquad P_h = \sum_{j=1}^{m} P_j \psi_j$$

represent the FEM approximate trial functions. Similarly,

$$\widetilde{w}_h = \sum_{i=1}^{n} \widetilde{w}_i \zeta_i \quad , \quad \widetilde{q}_h = \sum_{i=1}^{m} \widetilde{q}_i \psi_i$$

denote the approximated test functions.

Substituting these approximations for the trial and test functions in the Eqs (3.17) to (3.20), the discretized system matrix can be written as

$$\underbrace{\begin{bmatrix} K^{11} & K^{12} & K^{13} & K^{14} \\ K^{21} & K^{22} & K^{23} & K^{24} \\ K^{31} & K^{32} & K^{33} & K^{34} \\ K^{41} & K^{42} & K^{43} & K^{44} \end{bmatrix}}_{A^*} \underbrace{\begin{bmatrix} \underline{U} \\ \underline{V} \\ \underline{P} \\ \underline{\theta} \end{bmatrix}}_{U^*} = \underbrace{\begin{bmatrix} \underline{F^1} \\ \underline{F^2} \\ \underline{F^3} \\ \underline{F^4} \end{bmatrix}}_{F^*}, \tag{4.21}$$

where, A^* is block matric, U^* is block vector, and F^* denotes the associated block vector for the R.H.S. In block matrix,

$$K_{ij}^{11} = \Delta_1 \int_\Omega \left(\frac{\partial \zeta_j}{\partial X} \frac{\partial \zeta_i}{\partial X} + \frac{\partial \zeta_j}{\partial Y} \frac{\partial \zeta_i}{\partial Y} \right) d\Omega + \int_\Omega \left(\sum_{j=1}^{n} U_j \zeta_j \frac{\partial \zeta_j}{\partial X} + \sum_{j=1}^{n} V_j \zeta_j \frac{\partial \zeta_j}{\partial Y} \right) \zeta_i d\Omega,$$

$$K_{ij}^{22} = \Delta_1 \int_\Omega \left(\frac{\partial \zeta_j}{\partial X} \frac{\partial \zeta_i}{\partial X} + \frac{\partial \zeta_j}{\partial Y} \frac{\partial \zeta_i}{\partial Y} \right) d\Omega + \int_\Omega \left(\sum_{j=1}^{n} U_j \zeta_j \frac{\partial \zeta_j}{\partial X} + \sum_{j=1}^{n} V_j \zeta_j \frac{\partial \zeta_j}{\partial Y} \right) \zeta_i d\Omega,$$

$$K_{ij}^{44} = \Delta_4 \int_\Omega \left(\frac{\partial \zeta_j}{\partial X} \frac{\partial \zeta_i}{\partial X} + \frac{\partial \zeta_j}{\partial Y} \frac{\partial \zeta_i}{\partial Y} \right) d\Omega + \int_\Omega \left(\sum_{j=1}^{n} U_j \zeta_j \frac{\partial \zeta_j}{\partial X} + \sum_{j=1}^{n} V_j \zeta_j \frac{\partial \zeta_j}{\partial Y} \right) \zeta_i d\Omega,$$

$$K_{ij}^{13} = \int_\Omega \left(\frac{\partial \psi_j}{\partial X} \right) \zeta_i d\Omega, \quad K_{ij}^{23} = \int_\Omega \left(\frac{\partial \psi_j}{\partial y} \right) \zeta_i d\Omega, \quad K_{ij}^{31} = \int_\Omega \left(\frac{\partial \zeta_i}{\partial X} \right) \psi_j d\Omega,$$

$$K_{ij}^{32} = \int_\Omega \left(\frac{\partial \zeta_i}{\partial X} \right) \psi_j d\Omega, \quad K_{ij}^{24} = \Delta_3 \int_\Omega \zeta_j \zeta_i d\Omega, \quad K_{ij}^{42} = -\Delta_5 \, \underline{\mathrm{V}} \int_\Omega \zeta_j \zeta_i d\Omega.$$

$$K_{ij}^{12} = K_{ij}^{14} = K_{ij}^{21} = K_{ij}^{33} = K_{ij}^{34} = K_{ij}^{41} = K_{ij}^{43} = 0.$$

Q_2 element having $3rd$ order accuracy in L_2-norm is used to discretize the velocity and temperature components where as to approximate the pressure term, P_1^{disc} element of $2nd$ order accuracy in the L_2-norm is considered. The discretized system linearized by using Picard method and then Gaussian elimination method has been used to solved the related linearized systems.

The convergence of solution is assumed when the relative residual for each dependent variable fulfils the following criteria,

$$\left| \frac{\Upsilon^{n+1} - \Upsilon^{n}}{\Upsilon^{n+1}} \right| \leq 10^{-6}$$

where, Υ, denotes the dependent variable U, V, P, θ and n represents the number of iteration.

4.3 Results and Discussion

Figure 4.1(a) to 4.3(a) illustrate the influence of radiation parameter Rd on the streamlines for different modes of convection. Flow consists of main cell formed above the blockage in forced convection and mixed convection regimes while in free convection the main cell is noticed around the blockage. Almost same pattern was noticed for all the streamlines for small values of Ri at 0.1, 1. Fluid flow is observed in an enclosure due to the movement of upper surface. When the Rd varies from 0.5 to 2, all the streamlines are densely distributed all over the blockage and clockwise recirculation occurs near the top moving lid. Moreover core of the vortex shifted towards the right side of upper wall of enclosure above the obstacle, which indicate that the fluid velocity decreases in this regimes and overall heat is transferred due to the convection.

In Figure 4.3(a) Richardson number raised up to 10, impact of moving wall is decreases due to augmentation of buoyancy force (natural convection) which carry great amount of energy from the hot lower wall. For different values of Rd from 0 to 2, all the streamlines are equally distributed all over the cavity and center of rotating eddy is obliquely stretched around the blockage towards the top right edge due to the upper moveable wall. Absolute values of maximum stream function increases which shows the denser flow in the enclosure is induced due to the dominant of conduction.

Figure 4.1(b) to 4.3(b) depict the impact of Rd on isotherms for all three cases

of convection ($Ri = 0.1, 1, 10$). For the forced ($Ri = 0.1$) and mixed convection ($Ri = 1$) regimes, isotherms shows same behaviour in the cavity. Isotherms are spread from left corner of cold upper surface towards the right corner of the hot bottom surface of cavity. As Ri approaches to 10 (see figure 4.3(b)), now buoyancy force plays its roles in the cavity. The boundary layer is relatively thick and very small core region occurs such that the isotherms become almost parallel to the hot bottom wall showing that most of the heat is transferred through the conduction. It should be noted that the temperature gradient in the hot lower surface and below the isothermal blockage are weakened with enhancing the radiation parameter Rd from 0 to 2, for all different modes of convection. There is an increase in the density due to ascending floating particles from the hot lower surface of enclosure, which incur the change in resistance of the descending of the fluid flow.

Figure 4.4(a) and 4.5(a) illustrate the effect of combined convection and natural convection ($Ri = 10$) for different values of temperature ratio parameter Nr on the streamlines. By augmenting the values of Nr there is no significant change noticed on the streamlines. For $Ri = 1$, the bottom hot wall and upper moving surface of cavity collectively takes part on the flow of fluid, so mostly streamlines are gathered above the blockage and parallel to the top moving surface. Moreover when buoyancy force ($Ri = 10$) is dominant on the flow and with the augmentation of temperature ratio parameter streamlines are spread around the obstacle overall in the cavity. Streamlines become parallel to the adiabatic vertical surfaces due to raised up of Nr which shows the higher magnitude of flow in thin zone.

Figure 4.4(b) and 4.5(b) depict the impact of Nr on isotherms for two modes of convection (combined and natural). For mixed convection ($Ri = 1$) with the variation in temperature ratio parameter, a mild change has been noticed on the isotherms, and isotherms gradually become parallel and converging towards the hot bottom wall. In free convection ($Ri = 10$) with change in Nr, isotherms are spread all over the cavity and shows that high thermal state of fluid, which is due to the gravitational force. Temperature gradient enhanced showed that conduction mode is dominant.

Figure 4.6(a) portray the influence of Rd on the Nu_{avg} for all of the three regimes of convection. Nv_{avg} having direct relation with thermal radiation parameter. Heat transfer is increased for all the case of convection but it is more highlighted for $Ri = 10$. Figure 4.6(b) explained that θ_{avg} is increased with thermal radiation but having opposite trend with the Richardson number.

Figure 4.7(a) and (b) illustrate that the average Nusselt number and average temperature as a function of Ha for various value of Rd. Figure 4.7(a) shows that the Nu_{avg} is enhanced by increasing value of Rd but reverse trend is observed with an increment in Hartmann number. As increasing Ha means that the Lorentz force is enhanced and it reduces the speed of flow. Average temperature is an increasing function of Rd while θ_{avg} decreases with raised up of Ha at a particular value ($Ha = 50$) beyond this value opposite trend observed (see Figure 4.7(b)).

Figure 4.8(a) and (b) depict the effect of Nr on the average Nusselt number and average temperature for different values of Ri(0.1, 1, 10). Nu_{avg} are linearly increasing with the augmentation of temperature ratio parameter Nr for all values of Ri and temperature distribution is an increasing function of Nr but decline with the enhancement of Ri in the cavity.

Influence of different physical parameters on Nu_{avg} is displayed in Figure 4.9(a). Increasing the values of Ha leads to the high resistance in the cavity which oppose the flow and reduce the rate of heat transfer so Nu_{avg} is decreasing function of Ha. From Figure 4.9(b) it can be noticed that by enhancing the Ha (0 to 50), average temperature falls in the cavity but after this an increment in the temperature has been observed, whereas with an enhancement of Nr, enhances the thermal state of fluid which is responsible for enhancement of temperature in the cavity.

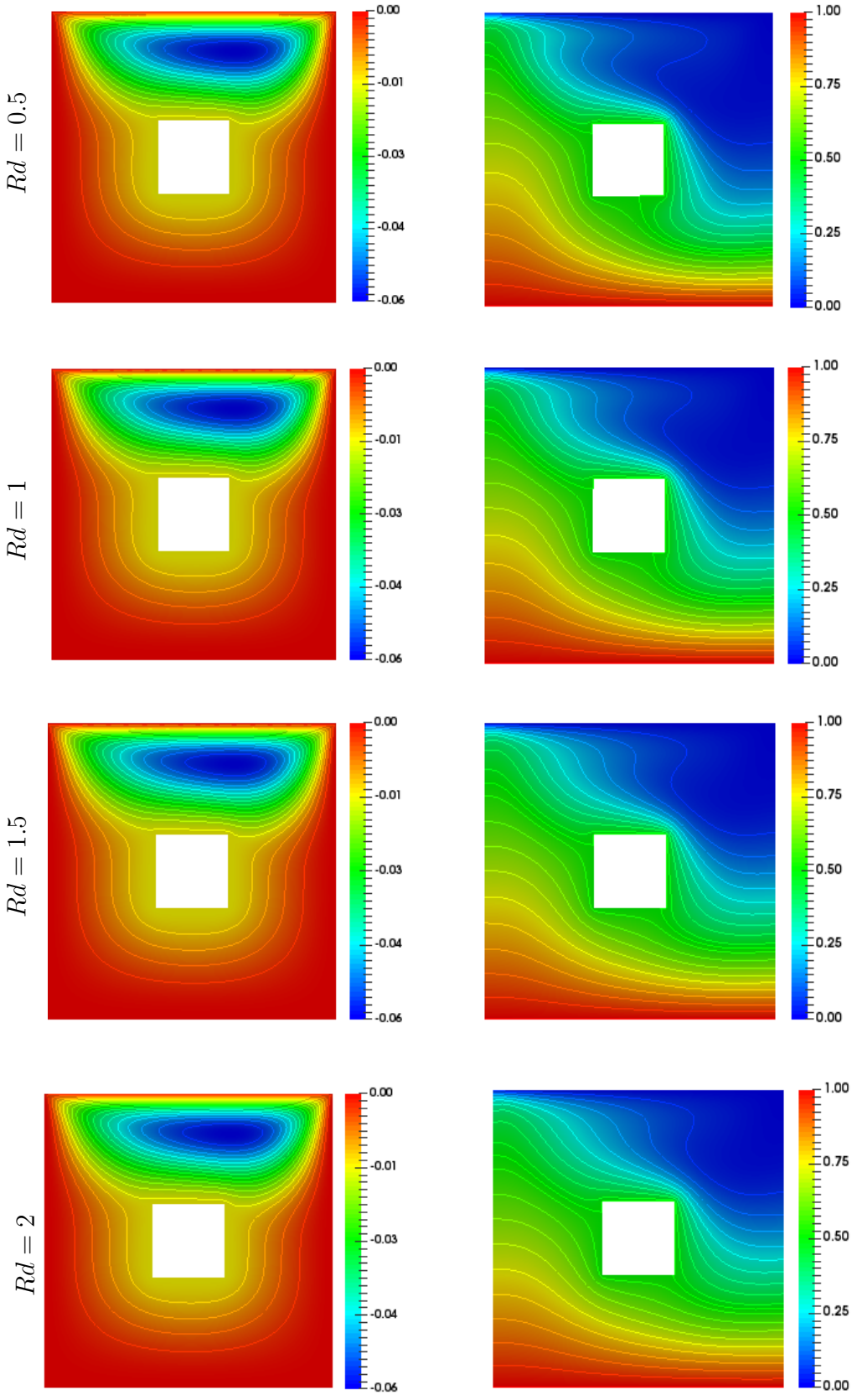

Figure 4.1: Streamlines (a) and isotherms (b) for different Rd at $Ri = 0.1$.

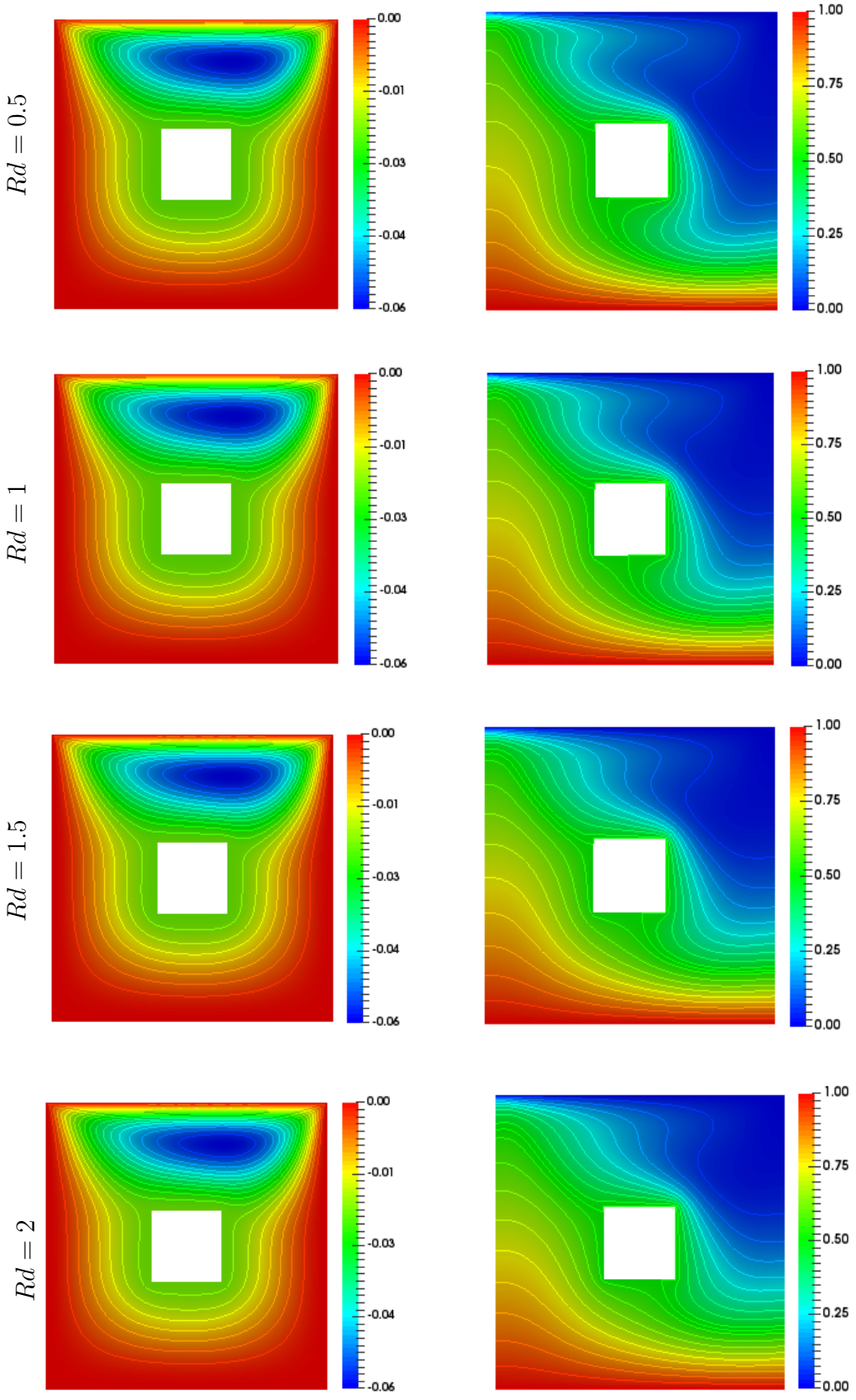

(a) (b)

Figure 4.2: Streamlines (a) and isotherms (b) for different Rd at $Ri = 1$.

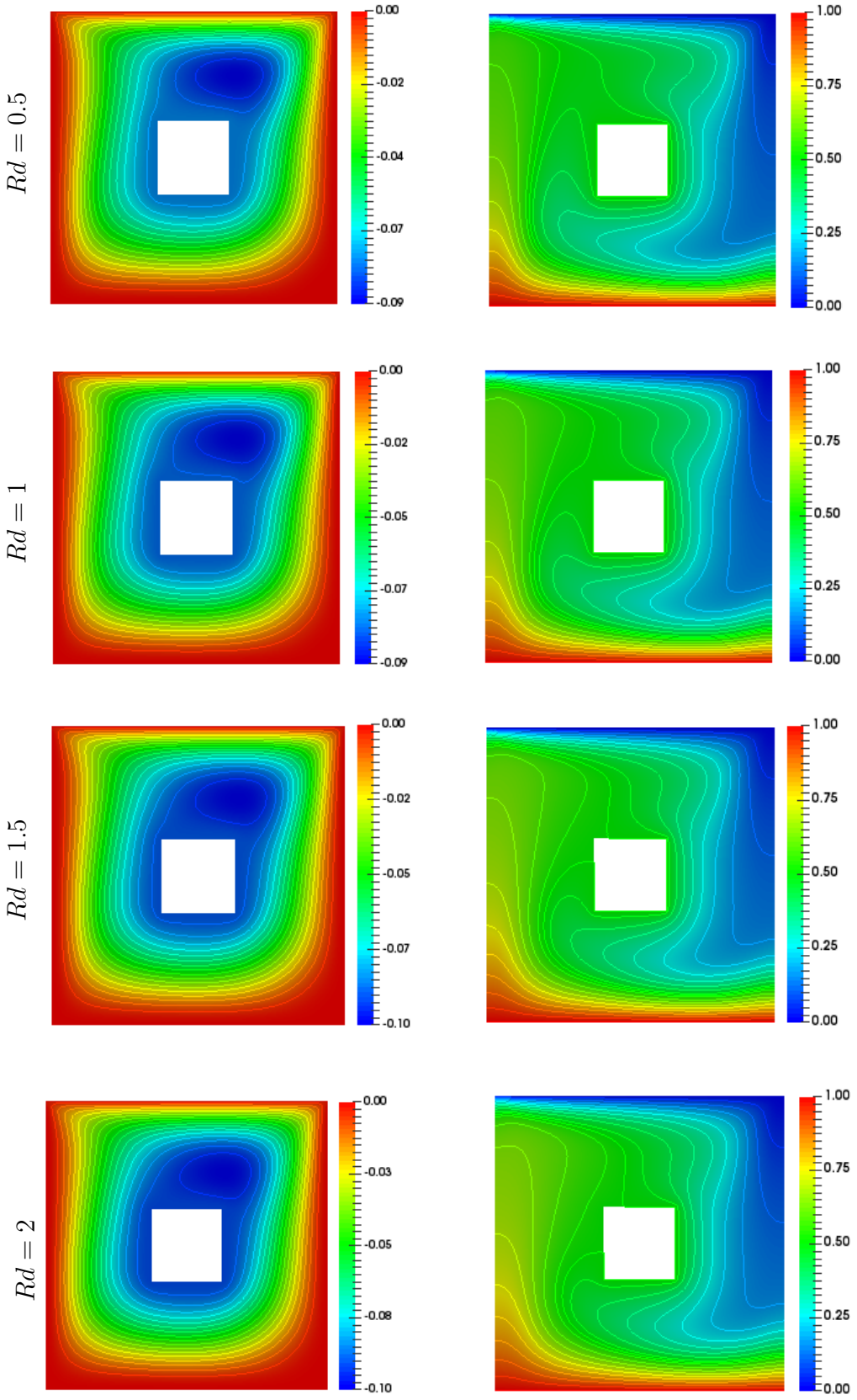

(a) (b)

Figure 4.3: Streamlines (a) and isotherms (b) for different Rd at $Ri = 10$.

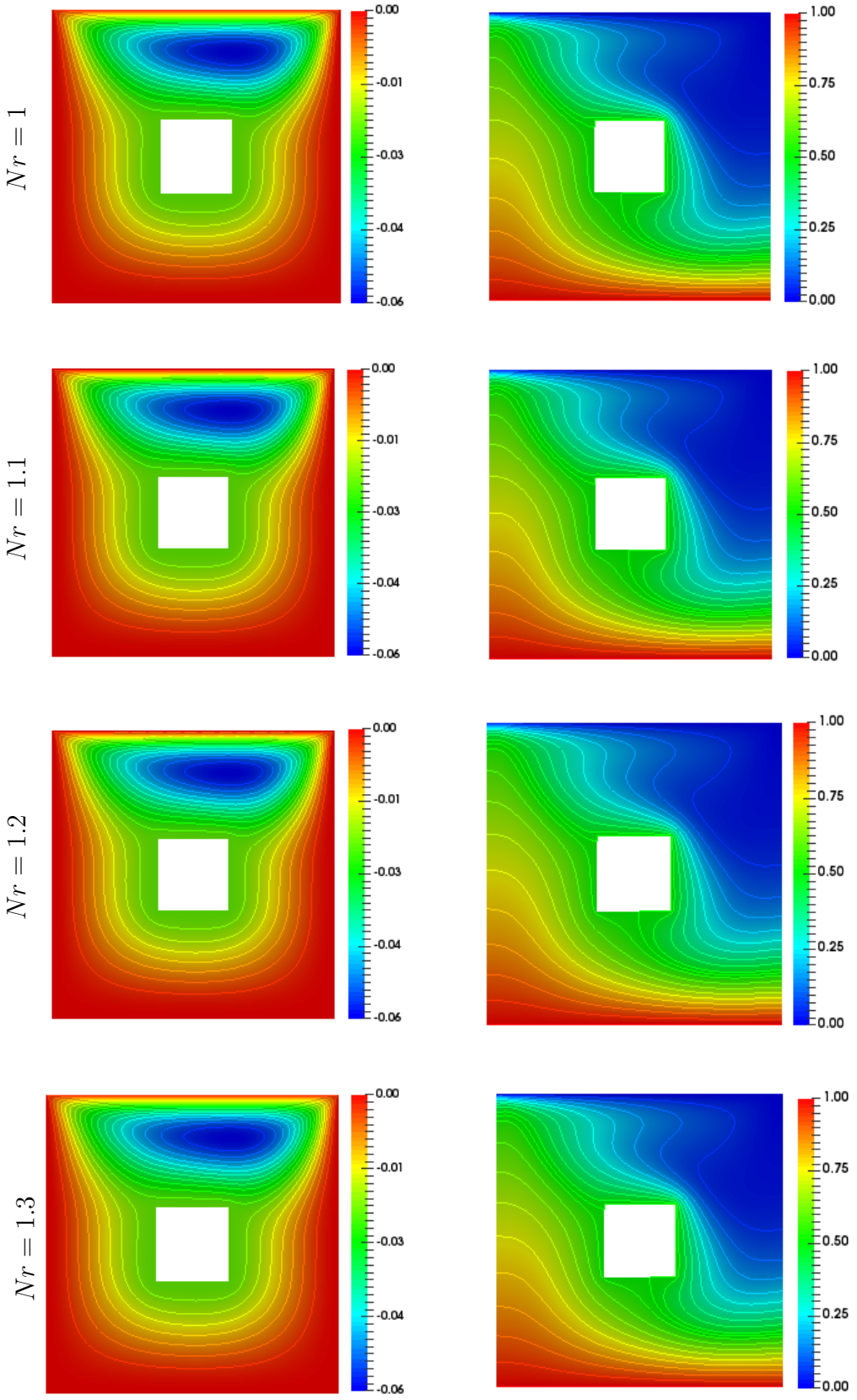

Figure 4.4: Streamlines (a) and isotherms (b) for different Nr at $Ri = 1$.

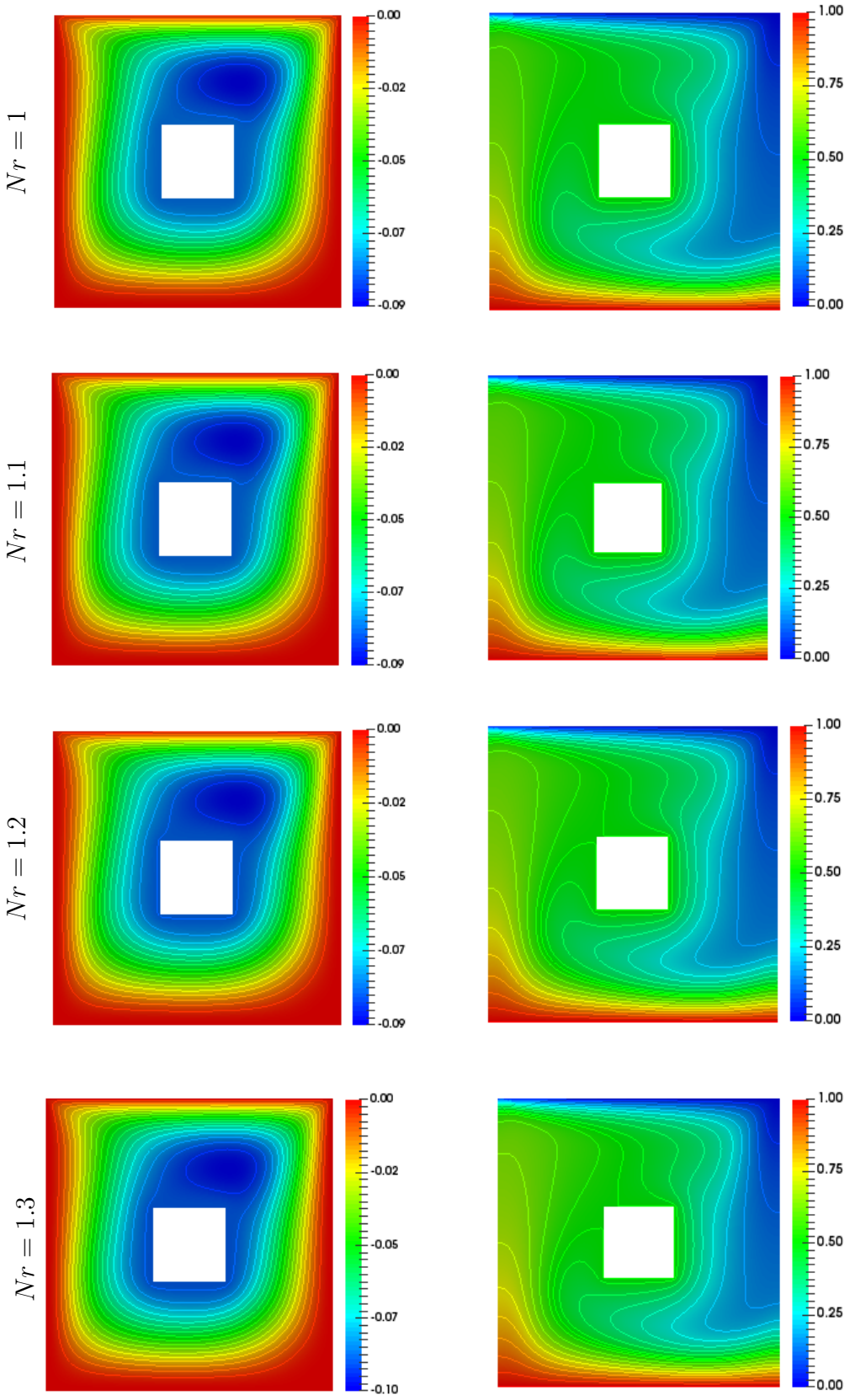

(a) (b)

Figure 4.5: Streamlines (a) and isotherms (b) for different Nr at $Ri = 10$.

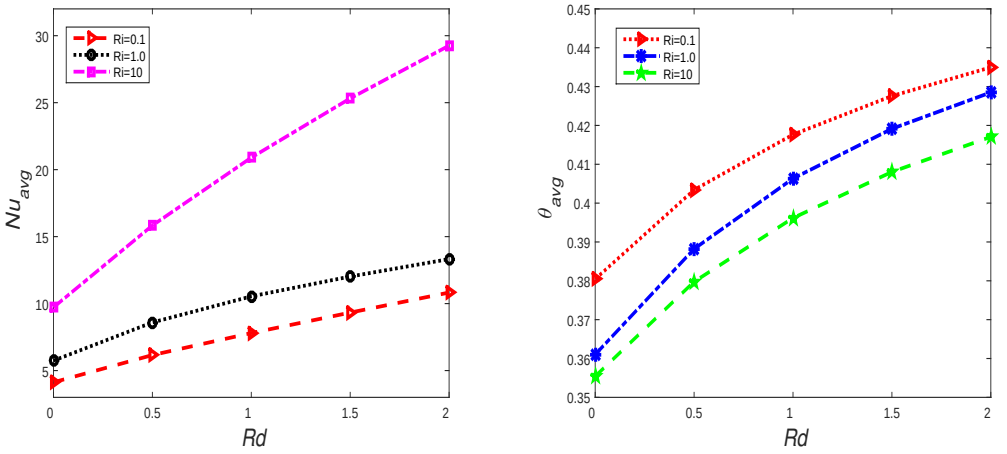

(a) (b)

Figure 4.6: Variation of Nu_{avg} and θ_{avg} as a function of Rd for different Ri.

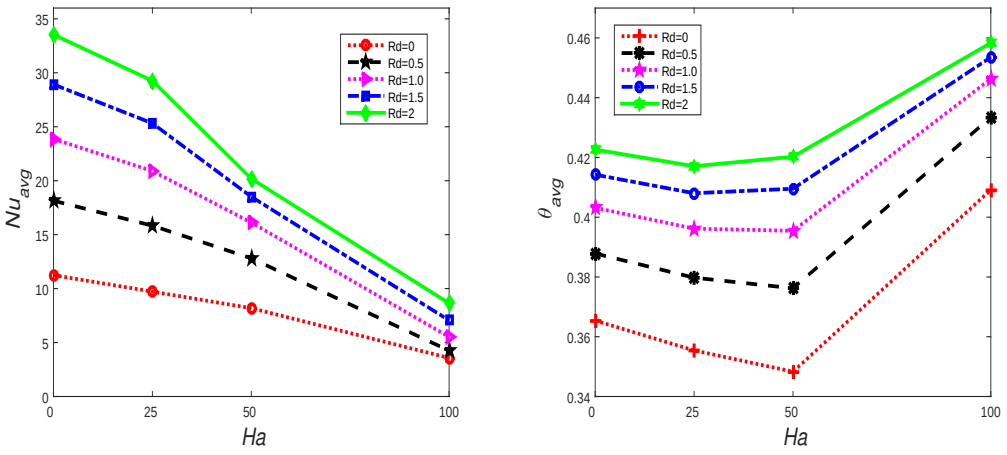

(a) (b)

Figure 4.7: Variation of Nu_{avg} and θ_{avg} as a function of Ha for different Rd.

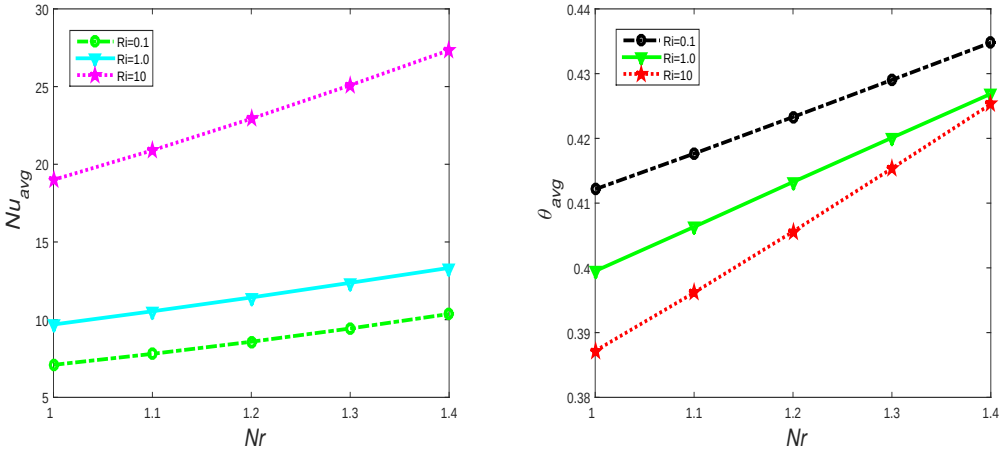

(a) (b)

Figure 4.8: Variation of Nu_{avg} and θ_{avg} as a function of Nr for different Rd.

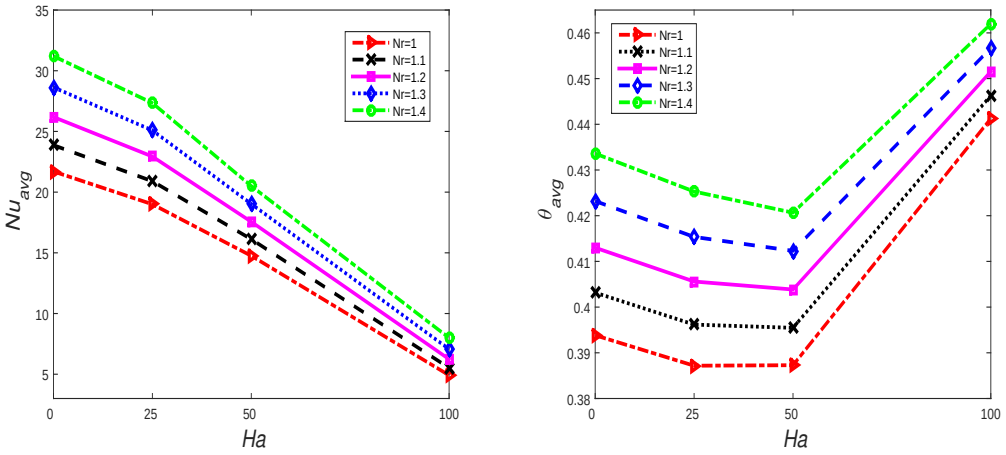

(a) (b)

Figure 4.9: Variation of Nu_{avg} and θ_{avg} as a function of Ha for different Nr.

Chapter 5

Conclusion

In this thesis, a two dimensional incompressible and steady MHD mixed convection flow under the leverage of non-linear thermal radiations is studied in a square enclosure. Both the vertical walls of the cavity are adiabatic whereas the upper surfaces exhibits the constant speed carrying the cold temperature and lower wall is subjected to the hot temperature. Moreover uniformly heated square cylinder is also kept in the middle of the enclosure. Fluid flow and heat exchange equations were first transformed into non-dimensional equations by applying suitable transformations and then discretized by using GFEM. The biquadratic element (Q_2) is used to discretized the velocity and temperature components and for pressure components ${P_1}^{disc}$ is used. The influence of pertinent parameters such as Hartmann number, Richardson number, Eckert number, Reynolds number and volume fraction of nanoparticles (ϕ) on the heat transfer and fluid flow have been extensively studied. The computational study of dimensionless temperature and velocity are analyzed with the help of isotherms and streamlines respectively, while graphical demonstration is also performed for the average Nusselt number.

In this study, the work of Mehmood *et al.* [27] is reviewed and extended with the concept of non-linear thermal radiations to assimilate the energy equation. The effect of thermal radiation parameter (Rd) and temperature ratio (Nr) on the heat transport phenomena and flow have been examined through the streamlines and isotherms. The average temperature and average Nusselt number are investigated

and plotted for the appropriate values of the parameters using MATLAB.
From the present study that has been numerically analyzed the following worthy points can be concluded,

- Increase in Nu_{avg} and θ_{avg} in cavity have been pronounced with the augmentation of nanoparticles of Al_2O_3 which shows that addition of nanoparticles in base fluid increase the phenomena of heat transfer.
- Raised up of thermal radiation has great influence on the maximum stream function values and mostly streamlines are spread in the cavity.
- Thermal radiation parameter and temperature ratio parameter both have positive impact on average Nusselt number and average temperature hence overall heat transfer rate is enhanced in the cavity.
- Nu_{avg} is an increasing function of Ri which is more pronounced at $Ri = 10$ due to dominant of buoyancy force.
- Increment of Ha shows the reduction in the rate of heat transfer and fluid flow due to the generation of Lorentz force in the opposite direction of flow.
- For certain values of Hartmann number, temperature gradient decline but after $Ha = 50$ average temperature rises in the cavity, because the greater values of Ha produces more resistance and temperature rises in the cavity.

5.1 Forthcoming Implementation

The study carried out in this thesis opens many gateways to new and innovative research directions, for example,

- The impact of ferrofluid (Fe_3O_4) on fluid flow and heat transfer can be investigated.
- Influence of porous media can be examined on the rate of heat transfer phenomena.

- Observing the influence of viscous dissipation incorporated into energy equation.
- Use of higher order finite element method for the spatial discretization.
- Analyzing the non-stationary behaviour of flow using the Galerkin discretization scheme for temporal discretization.

Bibliography

[1] E. Abu-Nada and A. J. Chamkha. Mixed convection flow in a lid-driven inclined square enclosure filled with a nanofluid. *European Journal of Mechanics-B/Fluids*, 29(6):472–482, 2010.

[2] M. M. Addini and S. G. Nassab. Combined mixed convection and radiation heat transfer in an obstacle wall mounted lid-driven cavity. *International Journal of Nonlinear Sciences and Numerical Simulation*, 17(6):277–289, 2016.

[3] S. E. Ahmed, M. Mansour, A. K. Hussein, and S. Sivasankaran. Mixed convection from a discrete heat source in enclosures with two adjacent moving walls and filled with micropolar nanofluids. *Engineering Science and Technology, an International Journal*, 19(1):364–376, 2016.

[4] A. M. Al-Amiri, K. M. Khanafer, and I. Pop. Numerical simulation of combined thermal and mass transport in a square lid-driven cavity. *International Journal of Thermal Sciences*, 46(7):662–671, 2007.

[5] A. A. Arani, S. M. Sebdani, M. Mahmoodi, A. Ardeshiri, and M. Aliakbari. Numerical study of mixed convection flow in a lid-driven cavity with sinusoidal heating on sidewalls using nanofluid. *Superlattices and Microstructures*, 51(6):893–911, 2012.

[6] N. Bakar, A. Karimipour, and R. Roslan. Effect of magnetic field on mixed convection heat transfer in a lid-driven square cavity. *Journal of Thermodynamics*, 2016, 2016.

[7] N. Bakar, A. Karimipour, and R. Roslan. Numerical study of mixed convection in a lid-driven cavity in the presence of internal heat generation/absorption. In *AIP Conference Proceedings*, volume 1830, page 020047. AIP Publishing, 2017.

[8] R. Bansal. *A Textbook of Fluid Mechanics*. Firewall Media, 2005.

[9] S. Bansal and D. Chatterjee. Magneto-convective transport of nanofluid in a vertical lid-driven cavity including a heat-conducting rotating circular cylinder. *Numerical Heat Transfer, Part A: Applications*, 68(4):411–431, 2015.

[10] M. Billah, M. Rahman, U. M. Sharif, N. Rahim, R. Saidur, and M. Hasanuzzaman. Numerical analysis of fluid flow due to mixed convection in a lid-driven cavity having a heated circular hollow cylinder. *International Communications in Heat and Mass Transfer*, 38(8):1093–1103, 2011.

[11] Z. Boulahia, A. Wakif, and R. Sehaqui. Numerical investigation of mixed convection heat transfer of nanofluid in a lid driven square cavity with three triangular heating blocks. *International Journal of Computer Applications*, 143(6), 2016.

[12] J. Buongiorno. Convective transport in nanofluids. *Journal of Heat Transfer*, 128(3):240–250, 2006.

[13] C. Cha and Y. Jaluria. Recirculating mixed convection flow for energy extraction. *International Journal of Heat and Mass Transfer*, 27(10):1801–1812, 1984.

[14] A. Chamkha, A. Rashad, T. Armaghani, and M. Mansour. Effects of partial slip on entropy generation and MHD combined convection in a lid-driven porous enclosure saturated with a Cu–water nanofluid. *Journal of Thermal Analysis and Calorimetry*, 132:1291–1306, 2018.

[15] T. Cheng. Characteristics of mixed convection heat transfer in a lid-driven square cavity with various richardson and prandtl numbers. *International Journal of Thermal Sciences*, 50(2):197–205, 2011.

[16] S. U. Choi and J. A. Eastman. Enhancing thermal conductivity of fluids with nanoparticles. Technical report, Argonne National Lab., IL (United States), 1995.

[17] N. S. Gibanov, M. A. Sheremet, H. F. Öztop, and N. Abu-Hamdeh. Effect of uniform inclined magnetic field on mixed convection in a lid-driven cavity having a horizontal porous layer saturated with a ferrofluid. *International Journal of Heat and Mass Transfer*, 114:1086–1097, 2017.

[18] N. Hamici and D. Sadaoui. Numerical study of mixed convection and thermal radiation in a square cavity with an inside inclined heater. *S5-Couplages Thermo-Mécaniques*, 2017.

[19] S. Hussain, H. F. Öztop, K. Mehmood, and N. Abu-Hamdeh. Effects of inclined magnetic field on mixed convection in a nanofluid filled double lid-driven cavity with volumetric heat generation or absorption using finite element method. *Chinese Journal of Physics*, 56(2):484–501, 2018.

[20] A. W. Islam, M. A. Sharif, and E. S. Carlson. Mixed convection in a lid driven square cavity with an isothermally heated square blockage inside. *International Journal of Heat and Mass Transfer*, 55(19-20):5244–5255, 2012.

[21] R. Iwatsu and J. M. Hyun. Three-dimensional driven-cavity flows with a vertical temperature gradient. *International Journal of Heat and Mass Transfer*, 38(18):3319–3328, 1995.

[22] R. Iwatsu, J. M. Hyun, and K. Kuwahara. Mixed convection in a driven cavity with a stable vertical temperature gradient. *International Journal of Heat and Mass Transfer*, 36(6):1601–1608, 1993.

[23] C. Johnson. *Numerical solution of partial differential equations by the finite element method*. Courier Corporation, 2012.

[24] B. Karbasifar, M. Akbari, and D. Toghraie. Mixed convection of water-aluminum oxide nanofluid in an inclined lid-driven cavity containing a hot

elliptical centric cylinder. *International Journal of Heat and Mass Transfer*, 116:1237–1249, 2018.

[25] J. Kuneš. *Dimensionless Physical Quantities in Science and Engineering*. Elsevier, 2012.

[26] A. Malleswaran and S. Sivasankaran. A numerical simulation on MHD mixed convection in a lid-driven cavity with corner heaters. *Journal of Applied Fluid Mechanics*, 9(1), 2016.

[27] K. Mehmood, S. Hussain, and M. Sagheer. Mixed convection in alumina-water nanofluid filled lid-driven square cavity with an isothermally heated square blockage inside with magnetic field effect: Introduction. *International Journal of Heat and Mass Transfer*, 109:397–409, 2017.

[28] K. Mehmood, S. Hussain, and M. Sagheer. Numerical simulation of MHD mixed convection in alumina–water nanofluid filled square porous cavity using KKL model: Effects of non-linear thermal radiation and inclined magnetic field. *Journal of Molecular Liquids*, 238:485–498, 2017.

[29] H. F. Öztop. Combined convection heat transfer in a porous lid-driven enclosure due to heater with finite length. *International Communications in Heat and Mass Transfer*, 33(6):772–779, 2006.

[30] H. F. Öztop, K. Al-Salem, and I. Pop. MHD mixed convection in a lid-driven cavity with corner heater. *International Journal of Heat and Mass Transfer*, 54(15-16):3494–3504, 2011.

[31] H. F. Öztop and I. Dagtekin. Mixed convection in two-sided lid-driven differentially heated square cavity. *International Journal of Heat and Mass Transfer*, 47(8-9):1761–1769, 2004.

[32] R. Patra, S. Das, and R. N. Jana. Radiation effect on MHD fully developed mixed convection in a vertical channel with asymmetric heating. *J. Applied Fluid Mechanics*, 7(3):503–512, 2014.

[33] L. A. B. Pilkington. Review lecture. The float glass process. *Proceedings of the Royal Society of London. Series A, Mathematical and Physical Sciences*, 314(1516):1–25, 1969.

[34] M. Rahman, M. Alim, and M. Sarker. Numerical study on the conjugate effect of Joule heating and magnato-hydrodynamics mixed convection in an obstructed lid-driven square cavity. *International Communications in Heat and Mass Transfer*, 37(5):524–534, 2010.

[35] W. M. Rohsenow, J. P. Hartnett, Y. I. Cho, et al. *Handbook of Heat Transfer*, volume 3. McGraw-Hill New York, 1998.

[36] L. K. Saha, M. C. Somadder, and K. S. Uddin. Mixed convection heat transfer in a lid driven cavity with wavy bottom surface. *American Journal of Applied Mathematics*, 1(5):92–101, 2013.

[37] M. Sharif. Laminar mixed convection in shallow inclined driven cavities with hot moving lid on top and cooled from bottom. *Applied thermal engineering*, 27(5-6):1036–1042, 2007.

[38] M. Sheikholeslami, T. Hayat, and A. Alsaedi. MHD free convection of Al_2O_3–water nanofluid considering thermal radiation: a numerical study. *International Journal of Heat and Mass Transfer*, 96:513–524, 2016.

[39] M. A. Sheremet and I. Pop. Mixed convection in a lid-driven square cavity filled by a nanofluid: Buongiorno's mathematical model. *Applied Mathematics and Computation*, 266:792–808, 2015.

[40] C. Sivaraj and M. A. Sheremet. Natural convection coupled with thermal radiation in a square porous cavity having a heated plate inside. *Transport in Porous Media*, 114(3):843–857, 2016.

[41] M. Thompson and J. H. Ferziger. An adaptive multigrid technique for the incompressible navier-stokes equations. *Journal of Computational Physics*, 82(1):94–121, 1989.

[42] M. Waheed. Mixed convective heat transfer in rectangular enclosures driven by a continuously moving horizontal plate. *International Journal of Heat and Mass Transfer*, 52(21-22):5055–5063, 2009.

[43] X.-Q. Wang and A. S. Mujumdar. A review on nanofluids-part i: Theoretical and numerical investigations. *Brazilian Journal of Chemical Engineering*, 25(4):613–630, 2008.

[44] I. Zeghbid and R. Bessaïh. Mixed convection in lid-driven cavities filled with a nanofluid. *International Journal of Heat and Technology*, 33(4):77–84, 2015.

[45] G. Zheng, M. Ha, H. Yoon, and Y. Park. A numerical study on mixed convection in a lid-driven cavity with a circular cylinder. *Journal of Mechanical Science and Technology*, 27(1):273–286, 2013.